Decaying lava extrusion rate at El Reventador Volcano, Ecuador measured using high-resolution satellite radar

Article

Published Version

AGU PUBLICATIONS

JGR

Journal of Geophysical Research: Solid Earth

RESEARCH ARTICLE
10.1002/2017JB014580

Key Points:
- High-resolution satellite radar measures extruded lava volume at the andesitic El Reventador stratovolcano at 11 day to 10 month intervals
- The time-averaged lava extrusion rate decays gradually over the 4 year observation period
- We fit the extrusion rate with a model of a depressurising reservoir, with constant magma influx from below at rates less than 0.35 $m^3\ s^{-1}$

Supporting Information:
- Supporting Information S1

Correspondence to:
D. W. D. Arnold,
david.arnold@bristol.ac.uk

Citation:
Arnold, D. W. D., Biggs, J., Anderson, K., Vallejo Vargas, S., Wadge, G., Ebmeier, S. K., … Mothes, P. (2017). Decaying lava extrusion rate at El Reventador Volcano, Ecuador, measured using high-resolution satellite radar. *Journal of Geophysical Research: Solid Earth*, *122*. https://doi.org/10.1002/2017JB014580

Received 23 JUN 2017
Accepted 27 NOV 2017
Accepted article online 30 NOV 2017

Decaying Lava Extrusion Rate at El Reventador Volcano, Ecuador, Measured Using High-Resolution Satellite Radar

D. W. D. Arnold[1], J. Biggs[1], K. Anderson[2], S. Vallejo Vargas[3,4], G. Wadge[5], S. K. Ebmeier[1,6], M. F. Naranjo[3], and P. Mothes[3]

[1]COMET, School of Earth Sciences, University of Bristol, Bristol, UK, [2]U.S. Geological Survey, California Volcano Observatory, Menlo Park, CA, USA, [3]Instituto Geofísico, Escuela Politécnica Nacional, Quito, Ecuador, [4]LMV, Université Clermont Auvergne, Clermont-Ferrand, France, [5]COMET, Department of Meteorology, University of Reading, Reading, UK, [6]COMET, School of Earth and Environment, University of Leeds, Leeds, UK

Abstract Lava extrusion at erupting volcanoes causes rapid changes in topography and morphology on the order of tens or even hundreds of meters. Satellite radar provides a method for measuring changes in topographic height over a given time period to an accuracy of meters, either by measuring the width of radar shadow cast by steep sided features, or by measuring the difference in radar phase between two sensors separated in space. We measure height changes, and hence estimate extruded lava volume flux, at El Reventador, Ecuador, between 2011 and 2016, using data from the RADARSAT-2 and TanDEM-X satellite missions. We find that 39 new lava flows were extruded between 9 February 2012 and 24 August 2016, with a cumulative volume of 44.8M m^3 dense rock equivalent and a gradually decreasing eruption rate. The average dense rock rate of lava extrusion during this time is $0.31 \pm 0.02\ m^3\ s^{-1}$, which is similar to the long-term average from 1972 to 2016. Apart from a volumetrically small dyke opening event between 9 March and 10 June 2012, lava extrusion at El Reventador is not accompanied by any significant magmatic ground deformation. We use a simple physics-based model to estimate that the volume of the magma reservoir under El Reventador is greater than 3 km^3. Our lava extrusion data can be equally well fit by models representing a closed reservoir depressurising during the eruption with no magma recharge, or an open reservoir with a time-constant magma recharge rate of up to $0.35 \pm 0.01\ m^3\ s^{-1}$.

1. Introduction

The rate of lava extrusion at erupting volcanoes is a key parameter for tracking changes in magma flux, eruptive behavior, and associated hazards, through time (e.g., Cashman & Sparks, 2013; Fink & Griffiths, 1998; Walker et al., 1973). The lava extrusion rate exerts a critical influence on the length and extent of lava flows and can provide insight into the dimensions and depth of the volcanic reservoir and conduit (Harris et al., 2007; Poland, 2014; Walker et al., 1973). At long-lived eruptions, variations in extrusion rate may give an indication of changes to the volcanic plumbing system or magma supply rate, and potentially an estimation of when declining eruptions may finish (Gudmundsson et al., 2016; Harris et al., 2003; Wadge, Oramas Dorta, & Cole, 2006).

Variations in lava extrusion rate have been observed on timescales varying from minutes through to decades (supporting information Table S1). On timescales of minutes to days, these fluctuations are generally due to shallow processes involving magma supply to the surface through a conduit with physical properties that can vary with time (Anderson et al., 2010; Hautmann et al., 2013; Johnson et al., 2008; Nakada et al., 1999; Voight et al., 1998; Walter et al., 2013). Over longer timescales, variations are thought to be caused by processes involving magma supply from the lower crust or mantle (e.g., Dvorak & Dzurisin, 1993; Harris et al., 2003; Poland, 2012, 2014).

Many volcanoes erupt at rates that are constant when averaged over years or decades ($0.1-2\ m^3\ s^{-1}$), regardless of magma composition or tectonic setting, presumably because this is the constant long-term supply rate of melt buoyantly rising through the crust (Sheldrake et al., 2016; Wadge, 1982). Figure 1 and supporting information Table S1 show a compilation of previously measured time-averaged extrusion rates over a range

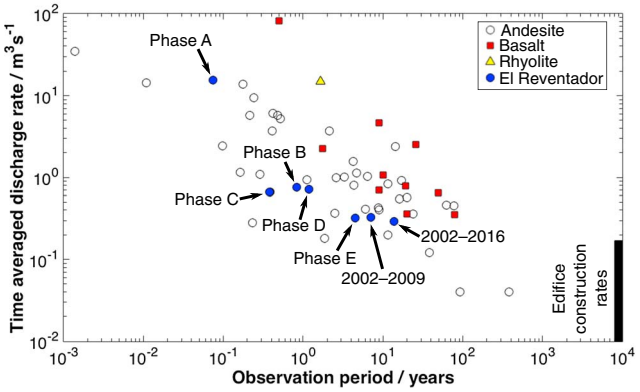

Figure 1. Time-averaged eruption rate from historical eruptions, plotted against the duration of observation period. Recent eruptive phases of El Reventador are labeled. Sources for the data are given in supporting information Table S1. The black bar shows the range of long-term volcanic edifice construction rates, which occur over timescales of 10^4 to 10^6 years (Thouret, 1999).

of measurement timescales. Longer measurement periods tend to give lower average extrusion rates, as pulses of high instantaneous lava flux are averaged out by intervening periods of much lower flux or quiescence intervals of no lava extrusion. We expect the trend of decreasing time-averaged discharge rate with observation time to plateau at increasingly longer observation times, as the observed extruded lava converges on the long-term magma supply rate, estimated to be 0.01 – 0.1 $m^3\ s^{-1}$ for most volcanoes from volcanic edifice construction rates measured over timescales of 10^4 years or longer (e.g., Thouret, 1999; Wadge, 1982).

Magma or volatiles entering or leaving a subsurface magma reservoir will cause a pressure change within the reservoir, which can lead to deformation of the ground surface (e.g., Dzurisin, 2003; Pinel et al., 2014). In an elastic crust, a volcanic eruption draining a single magma reservoir, with flow through the conduit proportional to reservoir pressure, will have an exponentially decaying extrusion rate and a deflation signal that also decays exponentially through time (e.g., Anderson & Segall, 2013; Dvorak & Okamura, 1987; Hreinsdóttir et al., 2014; Mastin et al., 2009).

Many volcanic eruptions are relatively short duration (weeks to months) and can typically be modeled by the depletion of one or more finite (closed) magma reservoirs beneath the volcano (e.g., Chaussard et al., 2013; Dzurisin, 2003; Rymer & Williams-Jones, 2000). The spatial and temporal pattern and magnitude of volcanic deformation can be modeled using simple analytical elastic half-space models (e.g., Mogi, 1958; Okada, 1985) or more complex numerical methods (e.g., Dieterich & Decker, 1975; Gottsmann et al., 2006; Hickey & Gottsmann, 2014) to constrain the source reservoir location and geometry. Kinematic deformation source models can be incorporated into physics-based models that include the physics of magmatic processes and can be used to naturally model the temporal evolution of deformation signals (e.g., Anderson & Poland, 2016; Anderson & Segall, 2013; Huppert & Woods, 2002; Segall, 2013). Models that do not include magma physics cannot naturally replicate this temporal evolution of the system (Segall, 2013).

Alternatively, volcanoes can behave as open systems, with persistent or frequent minor eruptions and degassing which can persist for decades, with little to no ground deformation (e.g., Biggs et al., 2014; Chaussard et al., 2013; Ebmeier et al., 2013a; Fournier et al., 2010; Moran et al., 2006; Pinel et al., 2011; Pritchard and Simons, 2002). The lack of observed ground deformation at these systems implies a lack of pressure change in the shallow system, possibly because of the high compressibility of volatile rich magmas, deep storage of melts that rise rapidly to the surface without intrusion in the upper crust, or temporal aliasing of deformation observations, which do not capture short-term transient deformation episodes (Biggs et al., 2014; Chaussard et al., 2013; Ebmeier et al., 2013a; McCormick-Kilbride et al., 2016).

Shorter-term transient deformation processes, associated with the magma conduit and lava dome, have been observed at long-lived andesitic dome forming eruptions, such as Soufriére Hills, Montserat, Colima, and Santiaguito (Johnson et al., 2008; Salzer et al., 2014; Sanderson et al., 2010; Voight et al., 1998; Walter et al., 2013). These transient processes occur on timescales of minutes to hours and are usually shallow and therefore only deform the area proximal to the active lava dome, making them difficult to detect with infrequent satellite observations, or distal ground-based monitoring instruments (Dzurisin, 2003; Segall, 2005).

Long-lived volcanic eruptions provide an ideal target for studying the evolution of open systems with time, the transitions between extrusive and explosive behavior and the underlying causes driving any changes, such as variations in magma supply rate, magma composition, and surface morphology (Cashman & Sparks, 2013; Segall, 2013; Watts et al., 2002). In this study, we use high-resolution radar satellite imagery to investigate the time-averaged lava extrusion rate, ground deformation and magma supply rate at the long-lived eruption of El Reventador, Ecuador.

2. El Reventador Background

El Reventador is a stratovolcano of basaltic andesite to andesitic composition, situated in the Cordillera Real approximately 90 km east of Quito (Figure 2b), and is one of the most active volcanoes in Ecuador, with more

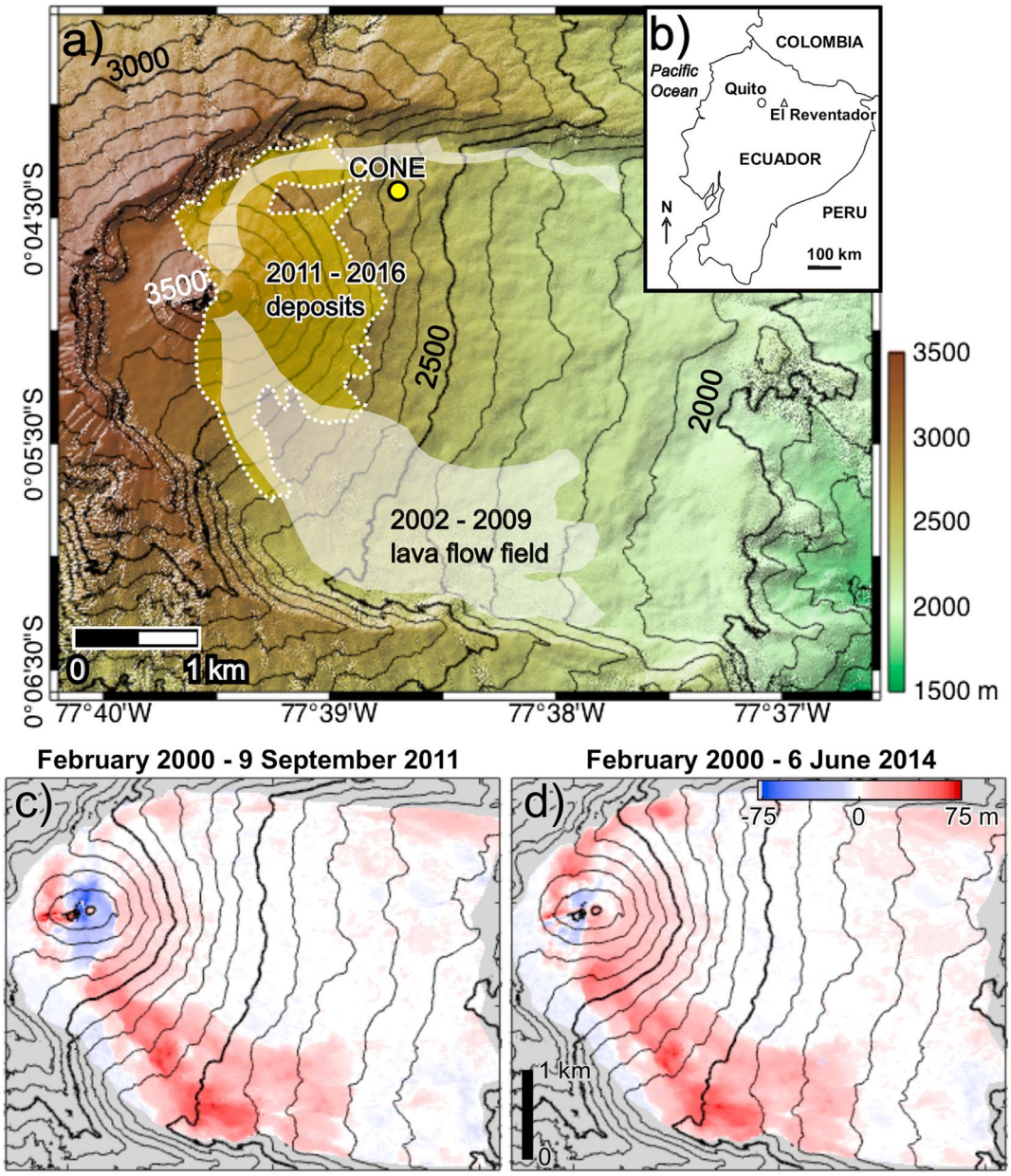

Figure 2. (a) Hillshaded digital elevation model (DEM) of El Reventador Volcano. Contours are at 100 m intervals, with bold contour lines every 500 m. The white polygons show the location of the 2002–2009 lava flow field mapped by Naranjo et al. (2016). The yellow polygon with white dotted outline shows the extent of the 2011–2016 volcanic deposits. These deposits include lava flows mapped from RADARSAT-2 amplitude data (Figure 4) and the area of topographic change between 9 September 2011 and 6 June 2014 from TanDEM-X imagery (Figure 5f). The yellow dot shows the location of the CONE seismic station, used by IG-EPN to detect explosions at El Reventador. (b) Location of El Reventador within Ecuador. (c, d) Cumulative height change of Phases A–E derived from TanDEM-X radar images. The topographic change is relative to the SRTM DEM. Negative elevation changes near the summit in Figure 2c were caused by the removal of material during the paroxysmal subplinian eruption on 3 November 2002 (Hall et al., 2004). This summit crater was almost completely filled by new lava erupted during Phase E (Figure 2d).

than 20 historical eruptive episodes since 1600 (Simkin et al., 1981). Following minor eruptive activity in the 1970s, the most recent eruptive period at El Reventador began with a subplinian explosion on 3 November 2002, which has been followed by semicontinuous eruptive behavior that is ongoing at the time of writing (Smithsonian Global Volcanism Program/Instituto Geofísico de la Escuela Politécnica Nacional (IG-EPN) activity reports).

The initial eruption began with little precursory surface or seismic activity and generated an ash plume that rose to 17 km and pyroclastic density currents which traveled up to 9 km from the vent (Hall et al., 2004). Subsequent eruptive behavior has been dominated by the extrusion of blocky basaltic andesite and andesitic lava flows, lava dome growth, and minor Strombolian explosions (Hall et al., 2004; Naranjo et al., 2016; Ridolfi et al., 2008; Samaniego et al., 2008). Petrological analysis of products from the 2002 eruption suggests that there was a single preeruptive reservoir with a top at 8 ± 2 km and a base at 11 ± 2 km (Ridolfi et al., 2008; Samaniego et al., 2008).

Naranjo et al. (2016) mapped and measured lava flows extruded in four phases (A–D) of activity between 2002 and 2009 at El Reventador, which each lasted 1–20 months and were separated by 18–24 months of quiescence (Figure 2a; Table 3 of Naranjo et al., 2016). They estimated total lava volumes of 90M ± 37M m^3 from field measurements, and 75M ± 24M m^3 from satellite remote sensing data. Based on visual, seismic and thermal observations of when lava flows are active, they present an average extrusion rate of 8.9 ± 3.7 m^3 s^{-1} for periods of lava extrusion. The long-term time-averaged discharge rate (including periods of repose) for Phases A–D was 0.33 ± 0.13 m^3 s^{-1} (Figure 1).

Based on satellite thermal observations from the MODVOLC algorithm, Phase E of the eruption at El Reventador began on 9 February 2012, following 23 months of minor activity (Wright, 2016). Phase E was preceded by at least 8 months of growth of a small lava dome at the summit of El Reventador (Global Volcanism Program, 2012). The first year of Phase E was characterized by mostly extrusive activity, followed by a step change in late 2012 or early 2013 to extrusive activity accompanied by numerous minor explosions that were detected by the CONE seismic station on the northeast flank of El Reventador (Figure 2). Due to periods of intermittent failure of the CONE station, the explosion record between 2012 and 2016 is incomplete. Phase E has lasted significantly longer than previous eruptive phases and is still ongoing as of June 2017. In this study, we focus on the time-averaged lava extrusion rate during Phase E, for which there exists a good archive of radar satellite imagery.

3. Surface Morphology

There are two approaches to measuring lava extrusion rate: instantaneous and time averaged. The first method records the instantaneous extrusion rate by observing the flux of lava out of a volcano or vent at a particular time and requires specific conditions in the field, such as the ability to measure the velocity of lava flowing in an open channel or tube of known dimension (e.g., Harris et al., 2007). The second approach involves measuring the time-averaged discharge rate, which is the change in erupted volume averaged over a given time period. Volume change at a volcano can be measured by comparing the difference in topographic surface in between two digital elevation models (DEMs) acquired at different times (e.g., Albino et al., 2015; Arnold et al., 2016; Bagnardi et al., 2016; Ebmeier et al., 2012; Harris et al., 2007; Kubanek et al., 2015; Poland, 2014; Xu & Jónsson, 2014; Wadge, 1983; Wadge, Oramas Dorta, & Cole, 2006). The time-averaged discharge rate is the sum of every pixel elevation difference, multiplied by the area of a raster grid cell, divided by the time period between DEM acquisitions.

Recent advances in remote sensing have provided numerous techniques for generating DEMs, which can be used to build up a time series of topographic change at active volcanoes (Bagnardi et al., 2016; Cashman et al., 2013; Diefenbach et al., 2013; Harris et al., 2007; Jones et al., 2015; Pinel et al., 2014; Schilling et al., 2008; Wadge, Voight, et al., 2014). Satellite radar is especially well suited to making repeat measurements of active volcanoes as it can cover a swath of 10–350 km at spatial resolutions of 1–10 m and repeat times of days to weeks, even at night or during cloudy conditions (Pinel et al., 2014; Wadge, Mattioli, & Herd, 2006).

3.1. Radar Methods

Variations in synthetic aperture radar (SAR) amplitude, caused by changes in surface roughness due to the emplacement of new volcanic deposits, can be used to map the extent of new lava flows (Dietterich et al., 2012; Wadge et al., 2011). Where the edges of lava flows are steeper than the radar incidence angle, the lava flow will cast a shadow from which no signal is returned to the satellite. The width of this radar shadow is proportional to the height of the object casting it, so can be used to measure the thickness of steep sided lava flows (Figure 3) using

$$h = \frac{w_{\mathrm{los}} \cos \phi}{\tan \theta} \tag{1}$$

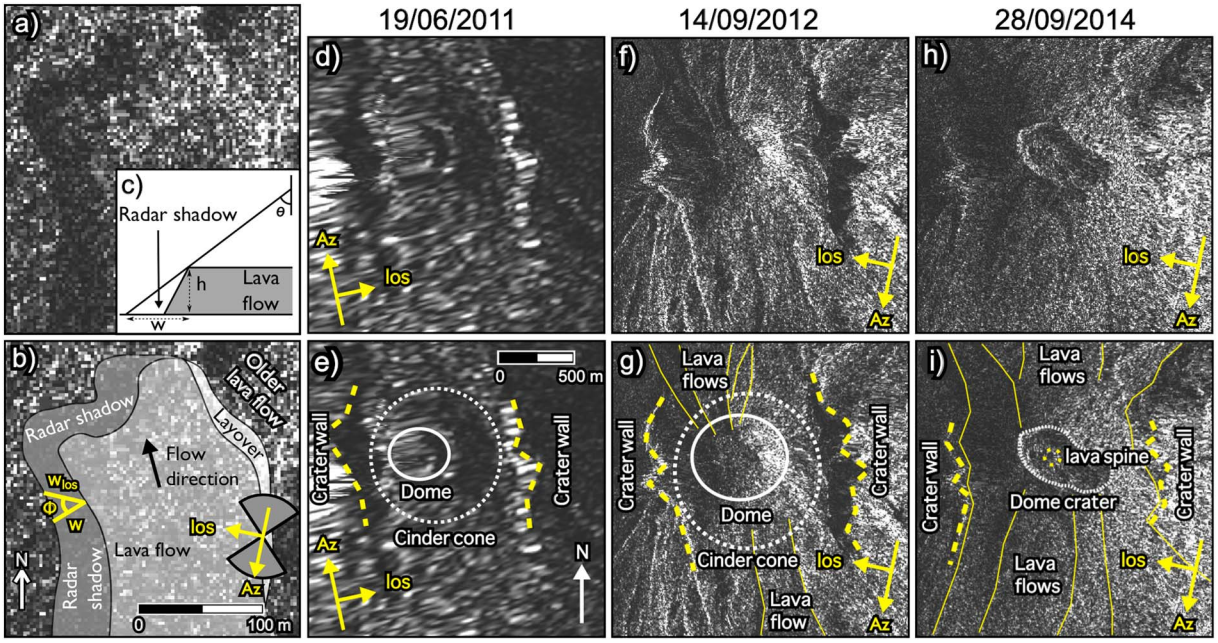

Figure 3. (a) RADARSAT-2 amplitude image of a lava flow which flowed from south to north on the northern flank of El Reventador. (b) Annotated amplitude image. The polygons give the extent of the flow, with the radar shadow to the west in dark grey and foreshortening and layover on eastern slopes facing the satellite in white. The truncated shadow cast by an older lava flow is visible in the northeast of the image. Az is the azimuth of the satellite direction of travel; los is the direction of radar line-of-sight; w_{los} is the width of the shadow measured in the satellite look direction; ϕ is the angle between w and w_{los}. The grey rose diagram shows the range of flow edge orientations which can be measured using the shadow method. (c) Schematic representation of the radar shadow method for measuring lava flow thickness. w is the width of the radar shadow, perpendicular to the flow edge; θ is the radar incidence angle; h is the height of the lava flow. (d–i) RADARSAT-2 amplitude images of the El Reventador lava dome, growing at the top of a cinder cone within a summit crater. Figures 3d and 3e were acquired in beam mode Wide 3, and Figures 3f–3i were acquired in beam mode Ultrafine 25 Wide 2. The extent of the dome is given by the solid white ellipse, the cinder cone by the dotted white ellipse, and the yellow dashed lines show the position of the west and east walls of the summit crater, which is breached to the north and south. Thin solid yellow lines in Figures 3e, 3g, and 3i highlight the edges of emplaced lava flows. Figures 3h and 3i show an ~ 24 m diameter lava spine extruded from the center of an explosion crater at the summit of the lava dome.

where h is the flow height, w_{los} is the shadow width in the radar line-of-sight direction, and ϕ is the angle between the radar line-of-sight direction and the line perpendicular to the lava flow edge, and θ is the radar incidence angle. This technique only works on flow edges which are orientated within ~ 45° of the satellite's direction of travel, in this case, a bearing of 147–237° for descending RADARSAT-2 data at equatorial latitudes (grey rose diagram on Figure 3b) (Wadge et al., 2011). Radar shadow thickness measurements can be used to estimate extruded lava volumes by assuming that lava flow thicknesses are constant across the whole flow and multiplying the thickness by the planimetric area of the flow.

The phase return of the radar signal can also be used to measure topography. For two satellites separated by a known distance, the difference in radar path length to the surface results in a phase difference in the interferogram formed between the image recorded at each satellite. The topography associated with the phase difference (e.g., Massonnet & Feigl, 1998) is given by

$$z = \frac{r\lambda \sin\theta}{4\pi B_{perp}} \Phi_{topo} \tag{2}$$

where z is the height, r is the range from the satellite to the ground surface, θ is the incidence angle, B_{perp}, the effective baseline is half the perpendicular distance between the two satellites (e.g., Kubanek et al., 2015), and Φ_{topo} is the topographic phase. For bistatic systems, where one sensor transmits and two sensors simultaneously record the same reflected signal, the phase contributions in an interferogram are due to the topography, the curvature of the Earth, and noise (e.g., Kubanek et al., 2015; Poland, 2014). The contribution from the Earth's curvature can be modeled and removed, leaving a phase difference which is only due to topographic height and noise, without any atmospheric phase contribution.

3.2. Data and Processing

We use satellite radar data from September 2011 to August 2016 to track changes in surface morphology associated with the eruption of El Reventador. A total of 32 images from the Canadian Space Agency (CSA) satellite RADARSAT-2 and 9 images from the Deutsches Zentrum für Luft- und Raumfahrt e. V. (DLR; German Space Agency) TanDEM-X mission were used. The satellite images are separated by time intervals ranging from 11 days to 10 months. RADARSAT-2 images from two different beam modes are used—25 acquired in mode Ultrafine 25 Wide 2, and 7 in mode Wide 3 (supporting information Table S2). TanDEM-X acquisitions over El Reventador ended in July 2014, while RADARSAT-2 images cover the whole period of interest from June 2011 until August 2016.

The TanDEM-X satellite pair operate in bistatic imaging mode, so the radar phase can be used to directly estimate the topography (equation (2)). In contrast, repeat-pass RADARSAT-2 interferograms contain phase contributions due to changes in atmospheric water vapor and ground deformation between image acquisitions, which make measurements of topographic change more difficult. We use the amplitude component of the RADARSAT-2 image to estimate the thickness of lava flows which have been active since the previous image acquisition (equation (1)), and the phase component to check for ground deformation at El Reventador.

We processed InSAR data using the interferometric SAR processor of the GAMMA software package (Werner et al., 2000). Bistatic TanDEM-X data were processed to construct DEMs of El Reventador at the time of each image acquisition using the methods described below.

Images were multilooked with four looks in range and azimuth directions to reduce phase noise. The Shuttle Radar Topography Mission (SRTM) 30 m DEM, acquired in February 2000, was linearly oversampled to 6 m and used as the reference DEM to estimate the topographic phase contribution for each interferogram (equation (2)). We find no evidence of artifacts associated with the oversampling in the residual topographic phase. Changes in topography since 2000 due to the eruption of El Reventador, which began in 2002, appear as residual phase contributions. For each interferogram, the vertical elevation change, z, can then be calculated using equation (2). Adding this height change to the SRTM topography gives a new DEM for each satellite acquisition. The DEMs produced from the TanDEM-X imagery have a pixel spacing of 6 m. The difference in elevation between two DEMs multiplied by the area of a single pixel (36 m^2) gives the bulk volume change due to the eruption between the two dates.

The amplitude component of each RADARSAT-2 image was geocoded from radar viewing geometry into latitude and longitude coordinates by cross correlation with a simulated amplitude image generated from a DEM, in order to map lava flow extents and estimate flow thicknesses (equation (1)). RADARSAT-2 amplitude images were processed at full resolution in order to preserve the minimum horizontal pixel spacing for measuring shadow widths. In order to minimize horizontal offsets in the amplitude imagery, all images were coregistered to a single master image and geocoded to the same DEM, which was generated from the TanDEM-X acquisition on 9 September 2011. The geocoded amplitude images have a horizontal pixel spacing of 2.5 m and were imported into the QGIS software package for analysis.

For each time step, we identified lava flows which had been active since the preceding image acquisition through visual comparison to the previous and subsequent images. Flow outlines were mapped, and the planar area of each flow was measured. Where possible, radar shadow widths were measured every 100 m downslope along each active lava flow and converted to thickness estimates using equation (1). The mean flow thickness was then multiplied by the flow area to give the bulk volume of each lava flow, and a total bulk lava volume for every time step.

For both the TanDEM-X and RADARSAT-2 data, bulk volume estimates are converted to a dense rock equivalent (DRE) volume. We assume the lavas erupted between 2012 and 2014 are petrologically similar to those erupted between 2002 and 2009, which were found to have a vesicularly of ~20% (Naranjo, 2013). We therefore multiply our bulk volume measurements by a factor of 0.8 to estimate DRE volumes.

3.3. Error Estimates

Both methods of estimating lava flow volume have associated uncertainties. The amplitude estimates assume that lava flow thicknesses measured at the edge of the flow are representative of the entire flow. Equation (1) assumes that the lava flow is traveling on a flat surface, which is not the case at El Reventador, where flows are descending an approximately conical edifice with numerous, radially oriented, eroded gulleys, and a complex preexisting lava flow field. In places where multiple flows are active between two image acquisitions,

flows active earlier in this period may be partially or wholly buried by younger flows. The area of the buried portion of the flow therefore has to be estimated, which adds additional uncertainty into the flow volume measurement. We assume shadow width measurements may be inaccurate by up to two pixels (5 m), which corresponds to a height error of between 2.9 and 4.5 m depending on the orientation of the flow edge relative to the satellite look direction (equation (1)). For flows where shadow measurements were possible along the whole length of the flow, the standard deviation in height measurements ranges between 1.5 m and 12.9 m, with a strong mode between 2 m and 3 m. We also assume flow area measurements are uncertain by variations in flow edge location of up to 5 m. Summing these errors for each time step give uncertainties in the amplitude volumes estimate of 15–40%, similar to uncertainties of 5–35% estimated by Naranjo et al. (2016) for field measurements of lava flow volume at El Reventador between 2002 and 2009.

The noise component of the topographic change derived from TanDEM-X phase measurements can be estimated by looking at the variation of measured height change in an area known to not be significantly affected by the eruption, and assumed to be at a constant elevation in all images. We use a 100 by 100 pixel box east of the summit as a reference area to give an estimate of the relative errors in the TanDEM-X derived DEMs. The reference area contains lava flows that were emplaced before the onset of the most recent eruptive period in 2002 and are not likely to be subsiding. For El Reventador, these errors are approximately ± 0.7 m for each pixel; therefore, we expect to be able to detect lava flows or pyroclastic deposits with a minimum thickness of 1 m. For each TanDEM-X derived volume change estimate, the cumulative errors from summing the uncertainty for each pixel give total uncertainties of 5–20%, approximately half the uncertainty associated with the shadow method.

3.4. Lava Volume

Using RADARSAT-2 amplitude imagery, we map 39 discrete lava flows between February 2012 and August 2016, which all appear to have originated from the summit lava dome; 18 of which descended down the north flank and 21 down the south flank (Figure 4 and supporting information Table S4). At least one active flow is present in 24 of the 25 scenes (supporting information Table S4) and all of the scenes show changes in the lava dome and summit crater morphology, showing that activity at El Reventador is apparently continuous when observed at intervals of 24 days. The total bulk volume of extruded lava flows during Phase E from 9 February 2012 until 24 August 2016 measured by RADARSAT-2 amplitude imagery is 56.0M $\pm$ 3.1M m^3, which gives a dense rock equivalent (DRE) of 44.8M $\pm$ 2.5M m^3 using a vesicularity of 20% (Naranjo, 2013). Lava dome volumes are over an order of magnitude less than lava flow volumes and are not included in this estimate (section 3.5, supplementary Tables S4 and S5).

Topographic change maps derived from TanDEM-X imagery show surface elevation changes of up to 80 m between September 2011 and June 2014 (Figure 5). The greatest cumulative lava flow thicknesses are on the north and south flanks of El Reventador, within 1 km of the summit. The cumulative bulk volume difference for Phase E up to 6 June 2014 was 33.3M $\pm$ 1.5M m^3 (26.7M $\pm$ 1.2M m^3 DRE).

RADARSAT-2 amplitude imagery and TanDEM-X phase observations both show the cumulative volume of lava erupted at El Reventador increased throughout 2012 to 2016, with no significant pauses in extrusion (Figure 6a). Lava volumes measured by the radar shadow method are in good agreement with the total volume change measured by DEM differencing for the 2 year period where both data are available (9 September 2011 to 6 June 2014)—33.1–35.8M m^3 from the shadow method compared to 33.3M m^3 from DEM differencing. The similarity between results from the different methods suggests that the erupted products are volumetrically mostly lava flows, with little contribution from ash or pyroclastic deposits (which do not have steep sides and are therefore difficult to measure with the shadow method).

The overall trend of the volume increase through time can be fit by an exponential with the form $V = A(1-e^{-Bt})$ (red line in Figure 6a, Table 1, and equation (3), or with the form $V = A(1 - e^{-Bt}) + Ct$ (blue line in Figure 6a, Table 1, and equation (9), where A, B, and C are all constants. The first equation is consistent with a closed depressurising magma reservoir without magma recharge, while the second equation represents the case of an open depressurising magma reservoir being resupplied at a constant volume flux C (Huppert & Woods, 2002; Segall, 2013). Both equations fit the data with a coefficient of determination, $R^2 > 0.99$ and similar root-mean-square error (RMSE) of 0.29M m^3 with recharge and 0.34M m^3 without.

The bulk time-averaged discharge rate derived from the gradient of the best exponential fit (without recharge) gradually decreases throughout the observation period from approximately 0.47 m^3 s^{-1} at the beginning

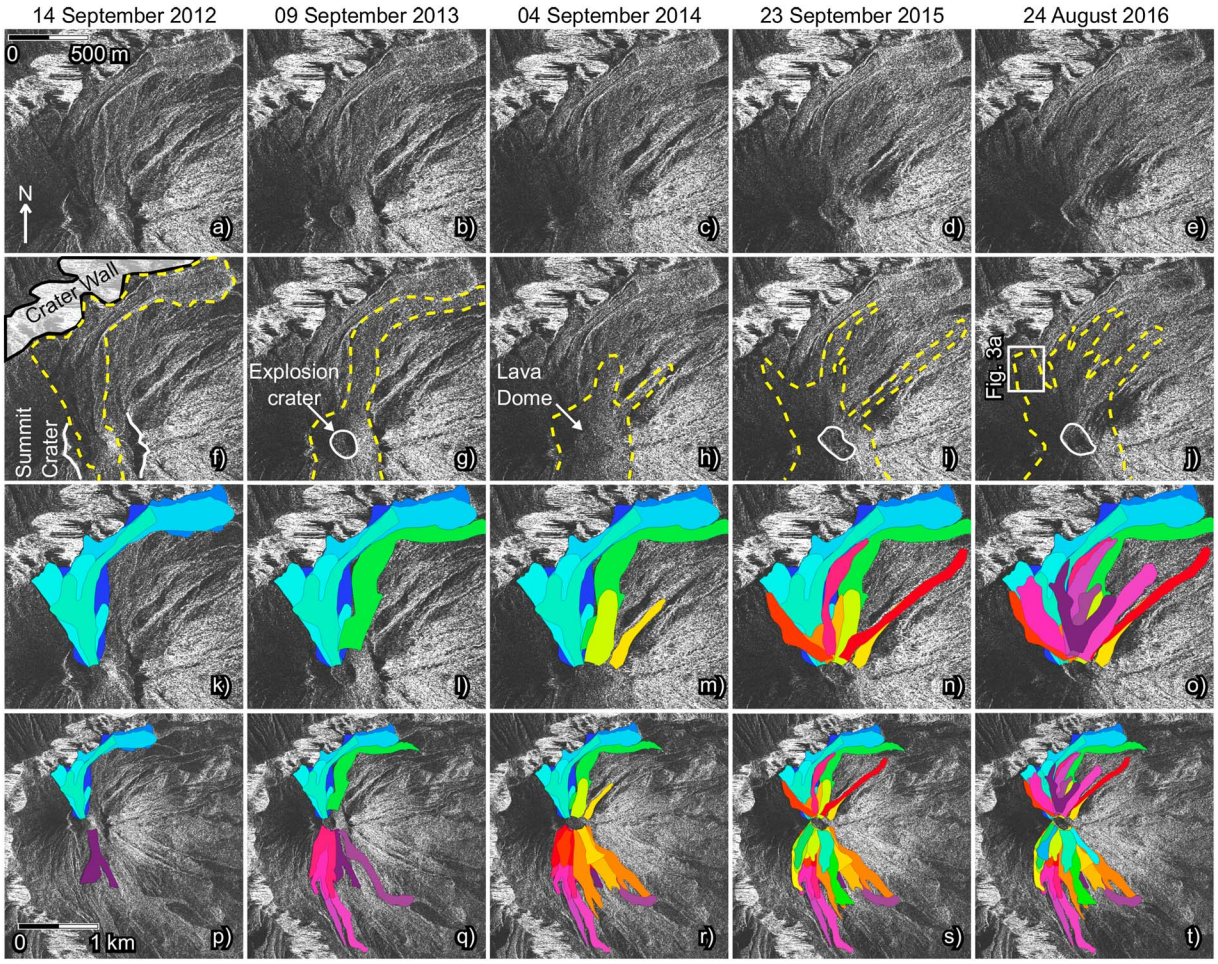

Figure 4. Extent of the lava flow field at El Reventador active between 6 March 2012 and 24 August 2016 mapped from RADARSAT-2 amplitude imagery. (a–e) RADARSAT-2 amplitude image of the summit and north flank of the active cone. Lighter colors indicate higher amplitude backscatter from slopes facing toward the ~ west looking satellite, while darker areas are slopes facing away from the satellite. (f–j) Yellow dashed lines outline the area of the lava flow field which has changed since the previous image due to new lava extrusion and (Figure 4f is the change from the first RADARSAT-2 acquisition on 6 March 2012). The solid white lines in Figure 4f shows the rim of the summit crater, which formed during the 3 November 2002 paroxysmal eruption. The white box in Figure 4j show the location of Figure 3a. White polygons in Figures 4g, 4h, and 4j outline craters in the summit lava dome formed by Strombolian explosions. (k–o) Cumulative lava flow field on the north flank of El Reventador. Individual lava flows are plotted with younger flows superimposed on older solidified flows. (p–t) Cumulative lava flow field at El Reventador between 2012 and 2016. Colors are schematic to differentiate separate lava flows.

of extrusion in February 2012 to 0.28 $m^3\ s^{-1}$ at the end of the observation period in August 2016. Alternatively, assuming constant magma recharge, the best fitting initial bulk time-averaged discharge rate was 0.77 $m^3\ s^{-1}$ in February 2012 and decreased more rapidly to 0.41 $m^3\ s^{-1}$ after 1 year and reached the recharge rate, C, of 0.36 $m^3\ s^{-1}$ by early 2014. In contrast, the best fitting linear gradient, without an exponential component, has a bulk rate of 0.44 $m^3\ s^{-1}$. This linear rate consistently underestimates the cumulative erupted volumes in 2012 to 2014, while overestimating the total volume throughout 2015 and 2016. Physics-based interpretations of these observations are discussed in section 5.

3.5. Dome Growth and Crater Morphology

At the start of our observation period in June 2011, El Reventador had a small lava dome that was growing at the top of a cinder cone that formed during 2009, located inside the summit crater formed by the 3 November 2002 paroxysmal explosion (Figure 3; Global Volcanism Program, 2012), which we estimate to be ~ 50 m deep (Figure 2c). From the RADARSAT-2 amplitude image acquired on 19 June 2011 (Figures 3d and 3e), we observe the lava dome to be elliptical and measure the length of the semimajor and semiminor axes (supporting information Table S5). We also use the shadow method to estimate the dome height and the depth of the summit crater which was ~ 50 m on 19 June 2011. We observe expansion of the dome through June to December 2011, consistent with aerial and field observations, which found a broadening of the dome between July 2011

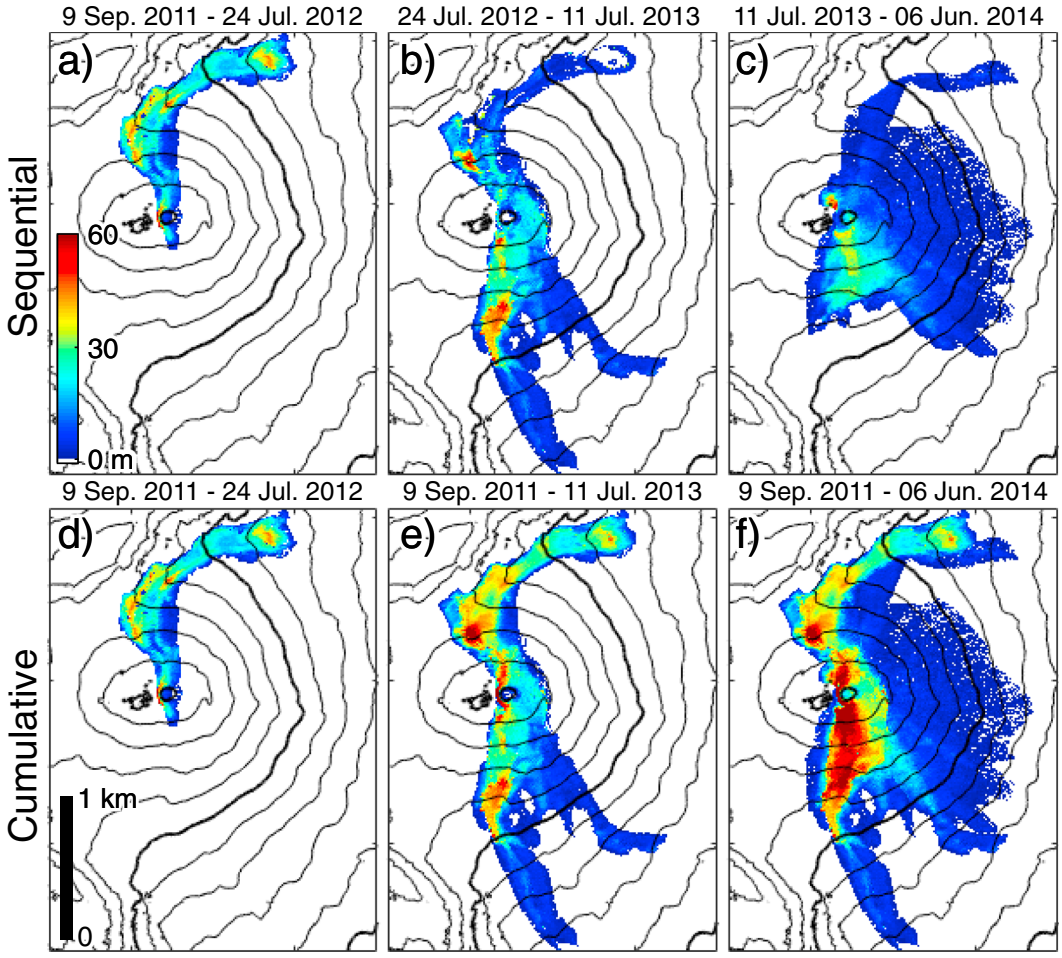

Figure 5. Topographic height change due to lava extrusion at El Reventador from DEMs constructed from TanDEM-X imagery. (a–c) Sequential elevation difference maps each spanning approximately one year. (d–f) Cumulative height change during Phase E of activity at El Reventador, relative to the earliest available TanDEM-X acquisition on 9 September 2011.

and January 2012 (Global Volcanism Program, 2012). After the start of lava flow extrusion in February 2012, the dome became partially covered by lava flows, which appear to originate from the summit of the dome, making size and shape difficult to determine; however, we are able to estimate the dome dimensions on 14 September 2012 (supporting information Table S5).

We treat the dome as the upper half of an oblate ellipsoid such that the bulk volume $V = 2\pi abc/3$, where a is the semimajor half axis, b is the semiminor half axis, and c is the dome height (Figure 6b). These dimensions yield a bulk dome volume of 0.33M m^3 in June 2011, growing to 0.48M m^3 in September, and 0.99M m^3 by the end of December 2011. The bulk time-averaged discharge rate for June to September 2011 was therefore 0.021 $m^3\ s^{-1}$, rising to 0.069 $m^3\ s^{-1}$ for September to December 2011, significantly less than the time-averaged rate after lava flow extrusion began in February 2012 (0.47 $m^3\ s^{-1}$). The volume of the dome increased to 1.47M m^3 by September 2012 at a rate of 0.023 $m^3\ s^{-1}$; however, the volume of lava flows extruded during this period was 1 order of magnitude greater (supporting information Table S4).

The SAR image on 25 March 2013 postdates the start of frequent minor explosive activity that occurred in early 2013 at El Reventador. A 120 m diameter crater is present at the center of the lava dome, and talus deposits are visible within the 2002 summit crater, piling up against the east and west crater rims. In the 31 January 2014 SAR image, pyroclastic deposits are visible in gullies on the east flank of El Reventador. These deposits were not present on 7 January 2014, suggesting that in the intervening 24 days, the base of the dome reached a height from which pyroclastic density currents were able to overtop the east wall of the 2002 summit crater. Shadow measurements of the eastern crater rim suggest up to 30 m of height change during this time period,

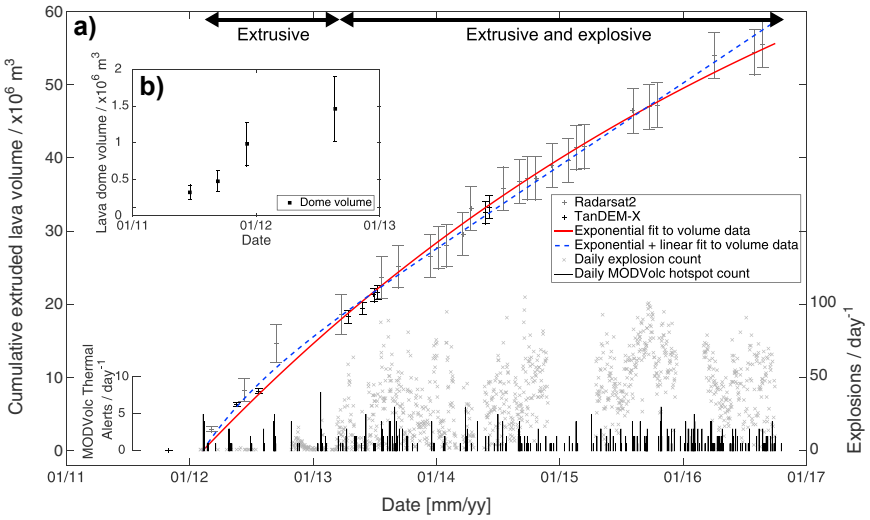

Figure 6. (a) Cumulative bulk volume of extruded lava at El Reventador. The middle-grey points are estimated from RADARSAT-2 shadow measurements. Black points are TanDEM-X phase measurements. The solid red and dashed blue lines give best fitting curves to the volume data. Pale grey crosses show the daily explosion count, recorded by the CONE seismic station located within the El Reventador crater. Gaps in the explosivity record, for example, in late 2012, 2014, early 2015, and early 2016, were due to intermittent failure of the CONE seismic station and do not indicate periods of no explosive activity. Vertical black bars show the number of daily hot spot pixels detected by the MODVolc algorithm. (b) Bulk volume of the lava dome at the summit of El Reventador, assuming the dome is a half ellipsoid. After 2013, explosions repeatedly remove part of the dome, hindering volume measurements.

although TanDEM-X measurements suggest less than 20 m elevation change between 11 July 2013 and 6 June 2014 (Figure 5c).

The dome morphology continued to change throughout 2013–2016, with a crater present at the top of the lava dome in 20 out of 22 RADARSAT-2 amplitude images after explosivity begins. In four of these images, there is a small area of paired radar layover and shadow, indicative of a feature with steep sides and without a flat top (Figure 3h). These features are all located in approximately the same area within dome summit craters and are 20–30 m in diameter and, from radar shadow widths, have a maximum height between 14 and 19 m above the crater floor. We interpret these features as lava spines—solidified lava that has been extruded out

Table 1
Parameters for Best Fitting Curves to Cumulative Volume Against Time at El Reventador

Phase	Type of fit	$A/\times 10^6$	B	C	RMSE/ $\times 10^6$ m^3
B	exponential	23	0.0076		3.1
B	exp + linear	8.9	0.12	0.47	2.1
B	power	1.9	0.42		2.4
D	exponential	25	0.010		4.7
D	exp + linear	14	0.21	0.30	1.7
D	power	4.8	0.27		3.1
E	exponential	98	0.00049		0.34
E	exp + linear	63	0.0060	0.36	0.29
E	power	0.15	0.80		0.25

Note. Exponential curves are of the form $V = A(1 - e^{-Bt})$, where A has units of m^3, B has units of days^{-1}, and $1/B \equiv t_c$. Exp + linear curves have the same form as the exponential curve, but with an additional linear term $+Ct$, where C has units of m^3 d^{-1} and represents a constant rate of magma reservoir recharge. Power law curves are of the form $V = At^B$, where B is dimensionless and A has units of m^3 d^{-B}. In all three equations V is the cumulative extruded lava volume in m^3 and t is the time since the start of the phase in days.

of a conduit by pressure from below, which were also observed at El Reventador between 2009 and 2012 (Global Volcanism Program, 2012).

From TanDEM-X derived DEMs, we estimate that between 9 September 2011 and 6 June 2014, the average elevation of the lava dome increased by 24 ± 4 m, while the distribution of talus deposits was constrained by the 2002 summit crater rim and increased in mean thickness by 59±11 m west of the dome and 39±2 m to the east. We observe minor negative topographic changes between some sequential TanDEM-X DEMs associated with crater formation at the summit of the lava dome; however, this volume loss is negligible compared to the overall volume increase. The largest volume removal we observe was between 28 May and 30 June 2013 with a volume decrease at the summit of ~0.15M m^3, while the net volume increase (including lava flows) for the same period was ~1.8M m^3.

RADARSAT-2 amplitude images from July 2014 to August 2016 show continued lava dome growth and talus build up against the 2002 summit crater walls, which by August 2016 had been almost completely in-filled. Images acquired after January 2014 suffer from geometric distortion near the summit of the lava dome due to changes in elevation since the acquisition of the TanDEM-X DEM on 9 September 2011, which was used to geocode all the satellite data into a common geometry for flow identification and analysis.

4. Ground Deformation and Modeling

4.1. Differential Interferometry

For both RADARSAT-2 and TanDEM-X data, repeat-pass differential interferograms were constructed using GAMMA to measure ground deformation at El Reventador (e.g., Dzurisin, 2003; Massonnet & Feigl, 1998). The topographic phase term was estimated using the 6 m DEM generated from earliest available TanDEM-X acquisition on 9 September 2011. The interferograms were filtered using an adaptive density filter (Goldstein & Werner, 1998), unwrapped using a minimum cost flow algorithm (Werner et al., 2002) and geocoded to the 2011 TanDEM-X DEM.

At El Reventador, loss of coherence is primarily caused by rapid vegetation growth in distal areas outside the recent lava flow field, and by resurfacing of the area proximal to the summit by lava flow extrusion, dome growth, rockfalls, and tephra and pyroclastic deposits (e.g., Ebmeier et al., 2014). Areas outside the 6 × 4 km El Reventador crater are almost entirely incoherent, while recent less-vegetated lava flows within the crater, up to 4 km from the active vent, are much more coherent. The flows show subsidence associated with cooling and compaction of the blocky lavas, a result previously observed in ALOS data from 2007 to 2011 (Fournier et al., 2010; Rivera Morales et al., 2016; Naranjo et al., 2016). The combined effect of lava subsidence in the near-field and incoherence in the far-field masks almost all potential edifice-wide ground deformation due to magmatic or hydrothermal processes underneath El Reventador.

4.2. Dyke Intrusion

We observe one period of ground deformation that we attribute to subsurface magmatic processes at El Reventador. The deformation is present in the ascending RADARSAT-2 interferogram between 9 March 2012 and 31 July 2012, and the descending interferogram spanning 6 March 2012 to 10 June 2012. In both interferograms, the deformation is limited to the area near the summit of the stratocone, just outside of the 2002 eruption crater, and the east and west flanks have an opposite displacement direction in the satellite line-of-sight. The ascending scene shows the west flank moved toward the east looking satellite, with a maximum magnitude of ~2 cm, while the east flank moved away from the satellite by up to 5 cm. In contrast, in the descending scene, the west flank has moved away from the west looking satellite by ~1 cm and the east flank moved ~1.5 cm toward the satellite (Figure 7). These observations indicate motion is dominantly horizontal, where the east flank moves to the east and the west flank moves west, consistent with a dyke opening underneath the summit. We assume that the deformation observed in both interferograms happened simultaneously in a short-duration event and that this dyke opening event occurred between 9 March 2012 and 10 June 2012.

The direction, magnitude, and spatial distribution of the deformation suggest that the source of the deformation is located underneath the summit of El Reventador, within the volcanic edifice. The shallow nature of the source, as demonstrated by the limited lateral extent of the deformation signal, suggests that the deformation is associated with the conduit supplying the eruption at the surface and that the dyke or conduit expanded a few weeks or months after lava flow extrusion began.

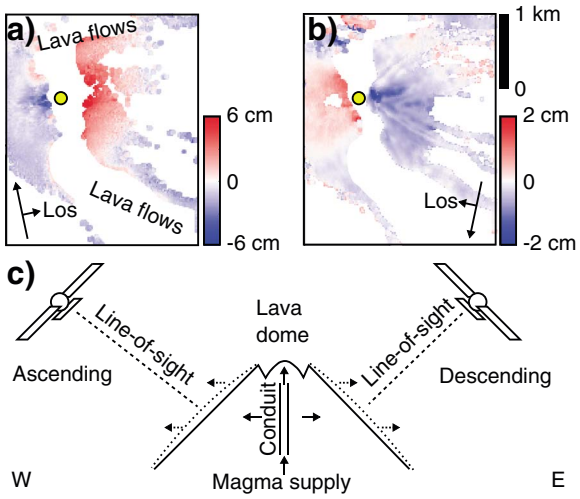

Figure 7. (a) Line-of-sight deformation (positive away from satellite, negative toward satellite) between 9 March 2012 and 31 July 2012 from ascending RADARSAT-2 data. (b) Line-of-sight deformation between 6 March 2012 and 10 June 2012. The yellow circle indicates the location of the lava dome. Recent lava flows have been masked to remove deformation associated with subsidence. (c) Schematic representation of the deforming edifice and satellite viewing geometries.

To investigate the geometry of this magmatic source for the March–June 2012 ground deformation at El Reventador, we performed a joint inversion on the two interferograms in which the deformation was observed using an elastic dislocation model (supporting information; González et al., 2015; Hooper et al., 2013; Okada, 1985). The lowest misfit model solution of this inversion is a small (100 × 600 m), shallow (base of dyke <1 km deep), vertical dyke oriented approximately north-south, opening by less than 1 m, and with a volume change of ~10,000 m^3 (Figure 8a). This solution is able to fit most of the deformation signal in the descending interferogram, but with significant and spatially complex residuals, and it substantially underestimates the magnitude of the deformation in the ascending interferogram. The misfit between the data and models is likely due to multiple factors that make the elastic half-space approximation unrealistic, including the following: the large (>1,000 m, Figure 2a) topographic relief near the summit of El Reventador; the complex geometry of the volcanic edifice, lava, summit crater, and lava flow field; and the likely nonelastic rheology of the shallow subsurface due to a combination of shallow hydrothermal activity and thermal and mechanical relaxation.

Despite the substantial uncertainties associated with the modeling method, the maximum intrusive volume change is still likely to be on the order of 0.01M m^3, which is approximately 2 orders of magnitude less than the extrusive lava volume for the same time period (~5M m^3), and therefore makes a negligible contribution to the overall magma budget. However, the expansion of the conduit may have caused a higher magma flux to the surface, resulting in an increase of the lava extrusion rate in the following months of 2012, as shown by the deviation of observed lava volumes from the best fitting exponential trend in middle to late 2012 (Figure 6a).

We do not find evidence for any other ground deformation episodes after the dyke opening in March to June 2012. Subsequent interferograms do not show a reversal of the deformation trend, suggesting that the pathway for magma to the surface remained open after June 2012. This conduit opening may explain the increased lava extrusion rate in June 2012 to March 2013, relative to the long-term exponential trend. Conduit opening would increase the cross-sectional area of the conduit, and therefore the volume flux at a given magma ascent velocity. There may be a correlation between the conduit opening and the increase in explosivity in early 2013; however, there is a 9–12 month lag between the deformation episode and the increase in explosive activity.

It is likely that there are shorter-term deformation processes associated with the conduit and lava dome at El Reventador, similar to those observed at Montserrat, Colima, and Santiaguio (Johnson et al., 2008; Salzer et al., 2014; Sanderson et al., 2010; Voight et al., 1998; Walter et al., 2013). Seismic records indicate up to 50 explosions per day at El Reventador (Figure 6a), giving an average repose period between explosions of ~30 min. Santiaguito Volcano in Guatemala exhibits similar ~30 min period explosivity, which are accompanied by up to 50 cm of uplift of the dome surface 1–2 s before the explosions (Johnson et al., 2008; Scharff et al., 2012). These transient processes occur on much shorter timescales than the observation frequency of satellite InSAR and are usually shallow and therefore only deform the area proximal to the active lava dome. Deformation observations within ~500 m of the summit of El Reventador are impossible after September 2012 due to loss of coherence caused by resurfacing of the ground surface by ashfall and pyroclastic deposits that were associated with the increase in explosive activity.

4.3. Constraints on Reservoir Volume Change

Interferograms from June 2012 onward do not contain any evidence of magmatic deformation at El Reventador. If we assume a magma reservoir geometry and place reasonable bounds on its location, we can put a lower limit on the minimum possible volume change that we would be able to detect given the level of noise in sequential interferograms (e.g., Ebmeier et al., 2013b). We consider the simple case of a volume change in a "Mogi" point source situated underneath the summit of El Reventador (Mogi, 1958). We consider the difference expected line-of-sight deformation in the area between 1 km and 2 km from the summit, which is mostly coherent in all interferograms. The average variance in line-of-sight deformation across the 23 RADARSAT-2 descending interferograms is ~ 3 mm, which we consider to be the detection threshold

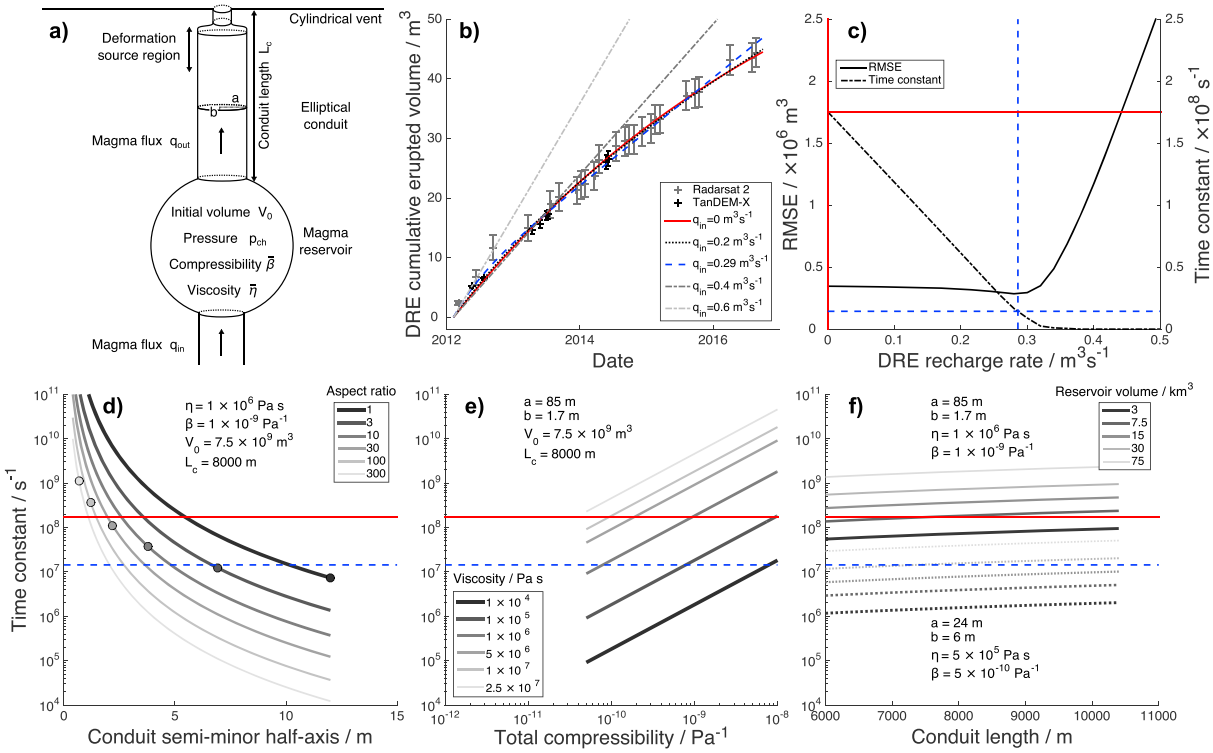

Figure 8. (a) Schematic representation of the magma reservoir used in the models, including the source region for the deformation signal discussed in section 4. (b) Relative fit of different models with constant recharge rates to the lava extrusion observations. (c) Misfit plot, showing the root-mean-square error (RMSE) of models with different constant recharge rate (solid black line) and the trade-off between recharge rate and time constant (dash-dotted black line). In all plots the solid red lines indicate the observed time constant (~2,000 days) assuming there is no magma recharge ($q_{in} = 0$), and the dashed blue lines give the best fitting time constant (~170 days) assuming magma recharge at a constant rate ($q_{in} = 0.29$ m^3 s^{-1}). Plots of t_c dependence on reservoir parameters: (d) conduit cross-section dimensions and aspect ratio, (e) compressibility and magma viscosity, and (f) conduit length and reservoir volume. In each plot, all other parameters are kept constant at the given values. In Figure 8f, the solid lines are plotted using the parameters given for a closed system, while the dotted lines are using the given open system parameters. The filled circles in Figure 8d give the value of b and t_c at given aspect ratios assuming the conduit cross-sectional area is equal to that of the lava spine observed on 28 September 2014.

for magmatic deformation at El Reventador. For a given reservoir depth, we assume we would be able to detect a reservoir volume change that resulted in 3 mm of line-of-sight range change at a horizontal distance of 1 km relative to at 2 km.

If we assume the 2012–2016 reservoir is at similar depths to the pre-2002 reservoir (7–12 km; Ridolfi et al., 2008; Samaniego et al., 2008), then the minimum volume change we would be able to detect is between 10M and 100M m^3 — a similar order of magnitude to the 44.8M ± 2.5M m^3 DRE that was extruded during this time period.

5. Models of the Magmatic System

Our data show eruption of lava at a slowly decreasing extrusion rate, with no significant detectable ground deformation. Here we introduce a simple physics-based model of a volcanic system and apply the model to our observations to attempt to constrain the physical characteristics of the magmatic system at El Reventador.

Physics-based volcano models provide a means of linking observations with underlying physical properties and processes (e.g., Anderson & Segall, 2011; Cashman & Sparks, 2013; Costa et al., 2007; Reverso et al., 2014; Sparks & Aspinall, 2004; Segall, 2013). These models may be used in quantitative inverse procedures to constrain properties of the volcanic system (Anderson & Segall, 2013). For example, a common observation is that within an individual volcanic eruption, including Phase E at El Reventador, lava extrusion rates are generally highest at the start of the eruption, and decrease through time as the eruption progresses (e.g., Anderson & Segall, 2011; Gudmundsson et al., 2016; Hreinsdóttir et al., 2014; Wadge, 1981, 1983). This behavior can be explained by balancing mass flux out of a magma reservoir in a purely elastic medium with Newtonian flow

along a conduit, modeled as a cylindrical pipe, which gives the equations for exponential decay of reservoir pressure change (e.g., Anderson & Segall, 2013; Hreinsdóttir et al., 2014; Huppert & Woods, 2002; Lu et al., 2003; Scandone, 1979; Wadge, 1981)

$$\Delta p(t) = \left(\bar{\rho} g L_c - p_{ch_0}\right)\left(1 - e^{-t/t_c}\right) \tag{3}$$

and the erupted volume

$$V_e(t) = V_0 \bar{\beta} \Delta p(t) \tag{4}$$

as the eruption progresses (Anderson & Segall, 2011; Mastin et al., 2008). In these equations, t is the time elapsed since the start of the eruption; Δp is the pressure change in the reservoir, relative to the overpressure above magmastatic pressure at the start of the eruption; p_{ch_0}. $\bar{\rho}$ is the depth-averaged magma density along the conduit; g is the acceleration due to gravity; L_c is the length of the conduit; V_0 is the initial reservoir volume; $\bar{\beta}$ is the overall compressibility, which is the sum of β_m, the magma compressibility, and β_{ch}, the reservoir compressibility; and t_c, the time constant, is given by

$$t_c = \frac{8\bar{\eta} V_0 \bar{\beta} L_c}{\pi R^4} \tag{5}$$

where $\bar{\eta}$ is the depth-averaged magma viscosity.

Ground deformation observations can be used to estimate reservoir location, geometry, and reservoir volume change or $V\Delta p$ (e.g., McTigue, 1987; Mogi, 1958; Okada, 1985; Yang et al., 1988), and the erupted volume can be measured directly (supporting information Table S1). Observations of ground deformation and erupted volume can therefore be used in conjunction with equations (3)–(5) along with information from other sources, such as petrology, rock mechanics, and gas fluxes, to constrain reservoir parameters (e.g., Anderson & Poland, 2016; Anderson & Segall, 2013; Costa et al., 2007; Hreinsdóttir et al., 2014; Kozono et al., 2013; Mastin et al., 2008; Melnik & Sparks, 2005; Reverso et al., 2014; Rivalta & Segall, 2008; Wadge, 1981). Here we present a physics-based model based on a pressurized reservoir in an elastic upper crust linked to the surface by a conduit (Figure 8a). We apply this model to our observations of erupted volume, temporal evolution of eruption rate, and lack of long-term ground deformation at El Reventador to estimate magma reservoir properties that cannot be directly observed, such as reservoir volume, pressure change, magma supply rate, reservoir compressibility, and volatile content (e.g., Anderson & Poland, 2016; Anderson & Segall, 2013; Mastin et al., 2008; Segall, 2013).

5.1. Reservoir Volume

For short-duration eruptions where there is negligible magma input, the initial volume of a magma reservoir V_0 can be estimated from the erupted volume V_e by considering conservation of mass (Anderson & Segall, 2014),

$$V_0 = -\frac{V_e}{\bar{\beta}\Delta p} \tag{6}$$

For simplicity, we assume that there is no density change in the magma between the reservoir and surface, and therefore, the dense rock equivalent volume extruded at the surface is the same as the volume that leaves the reservoir at the base of the conduit (e.g., Gudmundsson, 2016). The error introduced by this assumption should be small compared to the uncertainty in the parameters.

In order to estimate reservoir volume from the erupted volume, compressibility and reservoir pressure change must be estimated (equation (6)). Reservoir compressibility may be constrained based on knowledge of reservoir geometry and host rock rigidity; magma compressibility may be constrained a priori based on knowledge of typical magma properties in the crust, or else modeled directly as a function of the magma's various phases (Anderson & Segall, 2011; Mastin et al., 2008; Rivalta & Segall, 2008). Additionally, the ratio of reservoir and magma compressibility may be constrained a priori (Anderson & Poland, 2016) based on observations at other eruptions (e.g., McCormick-Kilbride et al., 2016). Rivalta and Segall (2008) define the ratio r_V between the erupted volume and the change in volume within a magma reservoir as

$$r_V = \frac{V_e}{\Delta V_{ch}} = 1 + \frac{\beta_m}{\beta_{ch}} = \frac{\beta_m + \beta_{ch}}{\beta_{ch}} \tag{7}$$

where ΔV_{ch} is the absolute value of the volume change of the reservoir. Theoretical values for r_V for degassed magmas range between 1.05 and 9; however, for volatile-rich magmas, r_V could be as high as 15 (McCormick-Kilbride et al., 2016; Rivalta & Segall, 2008).

We use the November 2002 paroxysmal eruption, which lasted approximately 45 min, as a short-duration eruption that can allow us to estimate the volume of the pre-2002 reservoir if we consider $q_{\text{in}} = 0$ (Hall et al., 2004). The bulk volume of erupted ash and pyroclastic flows was estimated to be ~350M m^3 (Hall et al., 2004), which we convert to a DRE volume of 150M m^3 using densities for dense rock, pyroclastic flow deposits, and tephra deposits that we assume are representative of andesitic dome forming eruptions, taken from Soufrière Hills, Montserrat (Wadge et al., 2010). From comparison to other volatile-rich systems, if we assume realistic upper bounds of 1×10^{-9} Pa^{-1} for $\bar{\beta}$ and −20 MPa for Δp (supporting information; Amoruso and Crescentini, 2009; Gudmundsson, 2016; Woods and Huppert, 2003), then V_0 must be greater than 7.5 km^3 . Alternatively, if we estimate upper bounds of 2.25×10^{-9} Pa^{-1} for $\bar{\beta}$ by using equation (7) and taking a maximum value of 1.5×10^{-10} Pa^{-1} for β_{ch} and 15 for r_V (Rivalta & Segall, 2008), then equation (6) gives $V_0 \geq 3.3$ km^3. The upper limit of the reservoir volume is poorly constrained; however, it is unlikely to be larger than approximately 150 km^3 (Gudmundsson, 2016).

The lack of deformation at El Reventador between 2012 and 2016 does not yield any additional constraints on reservoir volume, since ΔV_{ch} is a priori almost certainly less than V_e (section 4; McCormick-Kilbride et al., 2016; Rivalta and Segall, 2008). We therefore consider it reasonable to assume that the current reservoir has approximately the same volume as the 2002 reservoir, since the 150M m^3 erupted in 2002 represents at most 5% of the total reservoir volume, which has to be greater than ~3 km^3 (supporting information). We therefore assume the current magma reservoir has a volume greater than 3 km^3 with a poorly constrained upper limit.

5.2. Temporal Evolution of Extrusion Rate

Considering the temporal evolution of the erupted volume allows us to constrain additional parameters of the magmatic system (e.g., Anderson & Segall, 2011). If we model the reservoir recharge as time-constant, then following Huppert and Woods (2002) the change in reservoir pressure can be modeled by

$$\Delta p_{ch}(t) = -\left(p_{ch_0} - \frac{q_{in} t_c}{V_0 \bar{\beta}}\right)\left(1 - e^{-t/t_c}\right) + \frac{q_{in} t}{V_0 \bar{\beta}} \tag{8}$$

and the erupted volume by

$$V_e(t) = \left(V_0 \bar{\beta} p_{ch_0} - q_{in} t_c\right)\left(1 - e^{-t/t_c}\right) + q_{in} t \tag{9}$$

Equation (9) shows that for time-constant input flux, the erupted volume flux ($q_{\text{out}} \equiv \mathrm{d}V_e/\mathrm{d}t$) tends to the linear gradient q_{in} as $t \to \infty$. If $q_{\text{in}} = 0$ then equation (9) simplifies to the case for a closed system given by equation (4).

If we approximate the conduit as an elliptical pipe, then the time constant of the exponential decay is given by

$$t_c = \frac{4\bar{\eta}(a^2 + b^2) V_0 \bar{\beta} L_c}{\pi (ab)^3} \tag{10}$$

which simplifies to the case of a cylindrical pipe, equation (5), where $a = b = R$ (e.g., Anderson & Segall, 2011; Hreinsdóttir et al., 2014). The derivations for equations (8)–(10) are given in the supporting information.

If El Reventador behaves as a closed system ($q_{\text{in}} = 0$), the time constant of the eruption has six unknowns that trade off against each other (equation (10)); therefore, it is difficult to estimate any one parameter directly. Including a constant rate of magma supply adds an additional term for q_{in} that is independent of the time constant but will trade off against it (equation (9)). We are able to make measurements of $\Delta V_e(t)$ from our satellite radar observations, and by fitting equations (4) and (9) to our results, we can attempt to distinguish between a closed reservoir with no magma recharge or an open reservoir with recharge as potential models for the eruptive behavior at El Reventador. By calculating t_c from the fit to the data and considering sensible limits of a, b, $\bar{\beta}$, $\bar{\eta}$, V_0, and L_c (supporting information), we can investigate how these parameters trade off against each other and estimate likely values of each.

We estimate the best fitting model parameters for equation (9) using a nonlinear least squares method, evaluated with a trust-region algorithm using the MATLAB curve-fitting toolbox. We can assess the relative fit of the open and closed system models by comparing how the misfit between the data and model changes

as q_{in} increases from 0. Figure 8c shows the root-mean-square error (RMSE) between the extruded volume data for Phase E and the best fit to equation (9) as q_{in} changes. We find that the misfit at the best fitting solution (0.29 ± 0.01 m^3 s^{-1} DRE) is only slightly lower than the misfit at lower influx rates, including the closed system model, since q_{in} and t_c trade off against each other (equation (9)) and Figure 8c). We are therefore able to place only an upper limit on the recharge rate at El Reventador, which we find to be 0.35 m^3 s^{-1} DRE. This upper limit corresponds to the best fitting linear rate to the data (i.e., $t_c = 0$). The misfit with the data increases significantly at higher constant recharge rates (Figures 8b and 8c), and therefore, this upper limit of the recharge rate is well constrained.

5.2.1. Temporal Evolution of a Closed System

If we first consider the magma reservoir at El Reventador to be a closed system with no magma recharge during Phase E ($q_{in} = 0$) then this approach yields a good fit to the data (red line in Figure 6a) with a time constant t_c of 2,000 days, with 95% confidence limits between 1,700 and 2,600 days. Using equation (10), we can consider how conduit dimensions a and b, effective viscosity $\bar{\eta}$, compressibility $\bar{\beta}$, conduit length L_c, and reservoir volume trade off against each other if the time constant is known. Reasonable limits for these parameters are given in the supporting information.

The viscosity, compressibility, conduit length, and reservoir volume are all linearly proportional to the time constant, such that an increase in one parameter could be offset by an equivalent decrease by another (Figures 8e and 8f). The conduit length is constrained to 8 ± 2 km by petrological estimates of the depth of the reservoir top, and therefore, uncertainties on L_c are approximately 25% (Ridolfi et al., 2008; Samaniego et al., 2008); however, the other three parameters are all be subject to order of magnitude uncertainties.

Figure 8d shows the strong dependence of t_c on conduit dimensions and conduit cross-section aspect ratio r_A, which is 1 if the conduit is a cylindrical pipe and larger for dyke-like geometries. Taking the 24 m diameter spine on 28 September 2014 as an indication of the uppermost conduit dimensions gives a conduit with a cross-sectional area of 450 m^2. Using this area for the entire length of the conduit gives a strongly elliptical conduit with $a = 85$ m and $b = 1.7$ m and an aspect ratio of ~ 50 (filled circles in Figure 8d). However, given the uncertainties in V_0, $\bar{\eta}$, and $\bar{\beta}$, other conduit aspect ratios and geometries are possible.

5.2.2. Temporal Evolution of an Open System

If we instead consider the magmatic reservoir at El Reventador to be supplied with melt from below at a constant rate ($q_{in} > 0$), we can also model a good fit to the data (blue dashed line in Figure 6a), with $t_c = 170$ days and 95% confidence limits between 110 and 350 days. The time-averaged extrusion rate decreased gradually over the first year of lava extrusion and reached an effectively constant gradient by mid 2013. From equation (9) this linear gradient is equivalent to the constant influx rate, which gives $q_{in} = 0.36 \pm 0.01$ m^3 s^{-1} for Phase E at El Reventador. Assuming the lava flows have a vesicularity of 20% gives an influx rate of 0.29 ± 0.01 m^3 s^{-1} DRE.

The value of t_c we estimate for this open system model is approximately 1 order of magnitude lower than if there was no recharge. If we keep all other reservoir parameters the same as for the closed system, then it is impossible to fit the lower time constant given our limits on L_c and V_0 (Figure 8f). In order to fit the lower modeled time constant (blue dashed lines in Figure 8) the magmatic system at El Reventador would require either an order of magnitude lower compressibility or viscosity, or a more cylindrical conduit aspect ratio of ~ 4. A combination of these factors is likely (dotted lines in Figure 8f), which would give a value of $\bar{\beta}$ between 10^{-10} Pa^{-1} and 10^{-9} Pa^{-1}, $\bar{\eta}$ between 10^5 Pa s and 10^6 Pa s, and a conduit cross-section aspect ratio between 4 and 50, with a dyke width between 3.5 m and 12 m, respectively.

6. Long-Term Evolution and Magma Supply Rate

The time-averaged discharge rate at El Reventador between 2012 and 2016 shows a gradual decrease on the time scale of months to years. The average bulk eruption rate for the whole 4 year period is 0.39 ± 0.03 m^3 s^{-1}, which gives a DRE rate of 0.31 ± 0.02 m^3 s^{-1}, within error bounds of the average eruption rate between 2002 and 2009 of 0.33 ± 0.14 m^3 s^{-1} (Naranjo et al., 2016). These eruption rates at El Reventador are similar to the long-term average of 0.3–0.4 m^3 s^{-1} measured at other long-lived andesitic dome forming eruptions such as Santiaguito, Arenal, and Shiveluch (supporting information Table S1; Harris et al., 2003; Sheldrake et al., 2016; Wadge, Oramas Dorta, & Cole, 2006). Here we place these observations within the context of the earlier phases of eruptive activity at El Reventador.

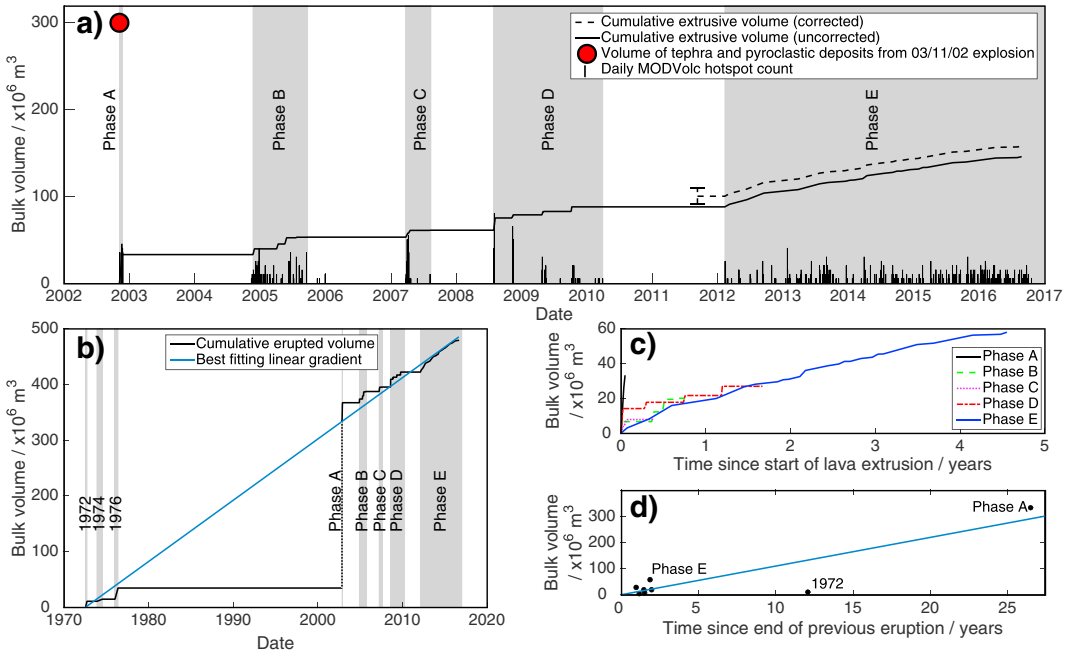

Figure 9. (a) Cumulative bulk volume of extruded lava flows at El Reventador since November 2002. The solid line plots the cumulative lava volume for Phases A to D from Naranjo et al. (2016), with RADARSAT-2 derived volumes for Phase E (supporting information Table S4). The dashed line shows the cumulative volume during Phase E, starting from the volume measured by the first TanDEM-X acquisition on 9 September 2011, plotted with 1 standard deviation error bars. Vertical black bars show the number of daily hot spot pixels detected by the MODVolc algorithm. Grey boxes show phases of lava flow extrusion. The red circle shows the estimated volume of magma erupted during the 3 November 2002 paroxysmal phase (Hall et al., 2004). (b) Cumulative bulk volume of extruded lava flows at El Reventador since November 1972. Volume data for 1972, 1974, and 1976 are from Hall et al. (2004), Phases A to D from Naranjo et al. (2016), and Phase E from RADARSAT-2 amplitude imagery (supporting information Table S4). The dotted line shows the estimated bulk volume erupted in the 3 November 2002 paroxysmal phase (Hall et al., 2004). The solid blue line shows the best fitting linear gradient to the data, which has a gradient of 0.35 $m^3\ s^{-1}$. (c) Cumulative volume of extruded lava flows for the five phases of lava extrusion at El Reventador since November 2002. (d) Bulk volume erupted during each phase against the time interval of quiescence preceding that phase. The blue line has the same gradient as the best fit solution to Figure 9b.

Naranjo et al. (2016) observed four distinct phases of activity at El Reventador between 2002 and 2009 (Figure 9a). The time-averaged discharge rate for Phase A was significantly higher than the subsequent phases, which all had rates similar to the start of phase E (Figure 9c). Phases B and D of lava extrusion appear to have a decrease in extrusion rate throughout the phase and, like Phase E, can be fit by exponential curves of the form $V = A(1 - e^{-Bt})$ or $V = A(1 - e^{-Bt}) + Ct$ (Figure 9c and equation 9), consistent with the behavior of a depressurising reservoir without and with magma recharge, respectively. Phases A and C are shorter in duration than the other phases, and there are not enough data to constrain a best fit curve. The curve for Phase E is less "stepped" in nature than the previous phases due to temporal aliasing of the satellite observations (Figure 9c). We are unable to determine exactly when a lava flow is emplaced between two satellite image acquisitions; therefore, we assume a linear rate of lava extrusion between the first and second image.

The data for Phase B, Phase D, and Phase E (2012–2016) are all better fit by exponential curves with a constant recharge rate than for no recharge, suggesting the resupply from either the mantle or a deeper reservoir is important at El Reventador (Table 1). From Table 1, and assuming a vesicularity of 20 % for all lavas, the best fitting linear DRE resupply rate was $0.38 \pm 0.29\ m^3\ s^{-1}$ for Phase B, $0.24 \pm 0.06\ m^3\ s^{-1}$ for Phase D, and $0.29 \pm 0.01\ m^3\ s^{-1}$ for Phase E. These recharge rates are all broadly similar given error ranges on the earlier phases, consistent with a constant supply rate of melt from below, although as with Phase E, we cannot distinguish between closed and open system models.

The extrusion rates for Phase B, Phase D, and Phase E can also be fit by a power law curve of the form $V = At^B$. For all three phases, the power law curve better fits the higher initial extrusion rate at the start of the eruptive phase than the best fitting no-recharge exponential solution. Phase B and Phase D are still better fit by an

exponential with recharge than a power law; however, the power law solution to Phase E has a lower misfit than either of the exponential solutions and would plot between the blue and red lines on Figure 6a.

While it is currently difficult to significantly distinguish between the three models, observations of future lava extrusion should allow better differentiation. As the eruption progresses, an exponentially decaying eruption will decrease extrusion rate more significantly than one following a power law, which would similarly decrease extrusion rate relative to the constant extrusive flux of an effectively open reservoir that is resupplied from deep. The power law equation could therefore be more representative of a magma reservoir which is exhibiting behavior between the end-member cases of a closed system without resupply and that of an open system with constant recharge. Such a system may be governed by nonlinear resupply rates, in which recharge from below is governed by the reservoir pressure (e.g., Anderson & Segall, 2011; Segall, 2013).

We use volume data from Hall et al. (2004) for the previous eruption of El Reventador during the 1970s in combination with data from Naranjo et al. (2016) and our results from 2011 to 2016 to estimate the average extrusion rate over the past four decades (Figure 9b). We find a best fitting linear gradient to the bulk lava volume of 0.35 $m^3\ s^{-1}$, with a 95% confidence interval of 0.33–0.38 $m^3\ s^{-1}$. This rate almost exactly matches the linear magma accumulation rate required to match the bulk volume erupted on 3 November 2002, assuming accumulation started after then end of the previous eruption in 1976. Assuming 20% vesicularity of erupted products would give a decadal DRE rate of $0.28 \pm 0.02\ m^3\ s^{-1}$, however, the majority of the bulk erupted volume in the paroxysmal phase were tephra deposits, which are generally lower density than lava flow deposits (e.g., Sparks et al., 1998; Wadge et al., 2010); therefore, 0.28 $m^3\ s^{-1}$ may be an upper bound on the long-term DRE extrusion rate. This long-term decadal extrusion rate is almost identical to the time-averaged rate of $0.27 \pm 0.07\ m^3\ s^{-1}$ DRE for lava flow extrusion postdating the 3 November 2002 explosion and also agrees well with the $0.29 \pm 0.01\ m^3\ s^{-1}$ linear magma supply rate derived from Phase E.

Since the range of estimated linear resupply rates between 0.2 and 0.4 $m^3\ s^{-1}$ matches well with the long-term DRE eruption rate at El Reventador, we infer that there has been no significant long-term increase in the volume of magma stored underneath El Reventador since 2002, implying a low likelihood of an eruption of similar magnitude to the November 2002 event. However, Figure 9d shows that the volume extruded in the 1972 eruption was much lower than expected given the preeruption repose period of 12 years. The approximately constant magma supply observed over the past four decades therefore appears to be different to the pre-1972 supply rate.

7. Conclusions

We use satellite radar data to measure the volume of extruded lava at El Reventador Volcano, Ecuador, between 2011 and 2016. We find a total DRE lava volume of $44.8M \pm 2.5M\ m^3$ was erupted between 9 February 2012 and 24 August 2016 at an average rate of $0.31 \pm 0.02\ m^3\ s^{-1}$, during a phase of lava extrusion that is still ongoing at the time of writing. This period of extrusion exhibited much more continuous activity than previous, shorter duration, eruptive phases at El Reventador. The average lava extrusion rate between February 2012 and August 2016 decreased gradually and can be equally well fit by models equivalent to a depressurising reservoir without magma recharge, or a reservoir that is being supplied with melt from below at a constant rate, which has an upper bound of $0.35 \pm 0.01\ m^3\ s^{-1}$.

We observe one period of ground deformation between 9 March and 10 June 2012, in which the pattern of ground deformation suggests a small, shallow, vertical, north-south oriented dyke opening underneath the summit. There are no other magmatic deformation events visible in interferograms covering 2012–2016, suggesting that the magma source is likely deep, large, highly compressible, or being resupplied from the lower crust or mantle. While there are large trade-offs between the reservoir volume and compressibility, we show that the reservoir is larger than 3 km^3 and the eruption is supplied through a conduit that is a dyke extending to a depth of 8 km. This dyke has a cross-section aspect ratio between 4 and 50, or lateral dimension between 12 m by 48 m and 3.5 m by 170 m.

We show the benefit of using radar amplitude imagery to supplement InSAR phase measurements of topographic change at erupting volcanoes. Such measurements could be usefully applied to other volcanic settings where radar phase measurements decorrelate, for instance, due to infrequent SAR acquisitions, resurfacing by volcanic activity or vegetation growth.

Acknowledgments
We thank M. Bagnardi, K. Cashman, M.E. Pritchard, and P. Segall for useful discussions and comments. We are grateful for constructive comments and suggestions from P. Tregoning, M. Poland, E. Montgomery-Brown, and two anonymous reviewers, which greatly improved the manuscript. D. A. is supported by a NERC studentship. J. B., G. W., and S. K. E. are supported by NERC COMET. J. B. and S. K. E. are supported by STREVA, and S. K. E. is supported by the Leverhulme Trust. The data used are listed in the supporting information. Satellite data were provided through the Committee of Earth Observation Satellites (CEOS) Volcano Pilot for Disaster Risk Reduction. RADARSAT-2 data were provided by the Canadian Space Agency and MacDonald Dettwiler & Associates Ltd. through proposal SOAR-geohazards-5297. TanDEM-X data were provided by Deutsches Zentrum für Luft- und Raumfahrt e. V. (DLR; German Space Agency) through proposal NTI_BIST7067. Any use of trade, firm, or product names is for descriptive purposes only and does not imply endorsement by the U.S. Government.

References

Albino, F., Smets, B., D'Oreye, N., & Kervyn, F. (2015). High-resolution TanDEM-X DEM: An accurate method to estimate lava flow volumes at Nyamulagira Volcano (D. R. Congo). *Journal of Geophysical Research: Solid Earth*, *120*, 4189–4207. https://doi.org/10.1002/2015JB011988

Amoruso, A., & Crescentini, L. (2009). Shape and volume change of pressurized ellipsoidal cavities from deformation and seismic data. *Journal of Geophysical Research: Solid Earth*, *114*, B02210. https://doi.org/10.1029/2008JB005946

Anderson, K., & Segall, P. (2011). Physics-based models of ground deformation and extrusion rate at effusively erupting volcanoes. *Journal of Geophysical Research*, *116*, B07204. https://doi.org/10.1029/2010JB007939

Anderson, K., & Segall, P. (2013). Bayesian inversion of data from effusive volcanic eruptions using physics-based models: Application to Mount St. Helens 2004–2008. *Journal of Geophysical Research: Solid Earth*, *118*, 2017–2037. https://doi.org/10.1002/jgrb.50169

Anderson, K., & Segall, P. (2014). Magma reservoir volumes and eruption forecasting, *Oral presentation at Euro. Geosci. Union Gen. Assem.*Vienna. abstract id. 15256.

Anderson, K., Lisowski, M., & Segall, P. (2010). Cyclic ground tilt associated with the 2004–2008 eruption of Mount St. Helens. *Journal of Geophysical Research*, *115*, B11201. https://doi.org/10.1029/2009JB007102

Anderson, K. R., & Poland, M. P. (2016). Bayesian estimation of magma supply, storage, and eruption rates using a multiphysical volcano model: Kīlauea Volcano, 2000–2012. *Earth and Planetary Science Letters*, *447*, 161–171. https://doi.org/10.1016/j.epsl.2016.04.029

Arnold, D. W. D., Biggs, J., Wadge, G., Ebmeier, S. K., Odbert, H. M., & Poland, M. P. (2016). Dome growth, collapse, and valley fill at Soufrière Hills Volcano, Montserrat, from 1995 to 2013: Contributions from satellite radar measurements of topographic change. *Geosphere*, *12*(4), 1300–1315. https://doi.org/10.1130/GES01291.1

Aspinall, W., Sigurdsson, H., & Shepherd, J. (1973). Eruption of Soufrière Volcano on St. Vincent Island, 1971–1972. *Science (80-.)*, *181*(4095), 117–124. https://doi.org/10.1126/science.181.4095.117

Bagnardi, M., González, P. J., & Hooper, A. (2016). High-resolution digital elevation model from tri-stereo Pleiades-1 satellite imagery for lava flow volume estimates at Fogo Volcano. *Geophysical Research Letters*, *43*, 6267–6275. https://doi.org/10.1002/2016GL069457

Belousov, A., Voight, B., Belousova, M., & Petukhin, A. (2002). Pyroclastic surges and flows from the 8–10 May 1997 explosive eruption of Bezymianny volcano, Kamchatka, Russia. *Bulletin of Volcanology*, *64*(7), 455–471. https://doi.org/10.1007/s00445-002-0222-5

Biggs, J., Ebmeier, S. K., Aspinall, W. P., Lu, Z., Pritchard, M. E., Sparks, R. S. J., & Mather, T. A. (2014). Global link between deformation and volcanic eruption quantified by satellite imagery. *Nature Communications*, *5*, 3471. https://doi.org/10.1038/ncomms4471

Cashman, K. V., & Sparks, R. S. J. (2013). How volcanoes work: A 25 year perspective. *Geological Society of America Bulletin*, *125*(5–6), 664–690. https://doi.org/10.1130/B30720.1

Cashman, K. V., Soule, S. A., Mackey, B. H., Deligne, N. I., Deardorff, N. D., & Dietterich, H. R. (2013). How lava flows: New insights from applications of lidar technologies to lava flow studies. *Geosphere*, *9*(6), 1664–1680. https://doi.org/10.1130/GES00706.1

Chaussard, E., Amelung, F., & Aoki, Y. (2013). Characterization of open and closed volcanic systems in Indonesia and Mexico using InSAR time series. *Journal of Geophysical Research: Solid Earth*, *118*, 3957–3969. https://doi.org/10.1002/jgrb.50288

Cigolini, C., Borgia, A., & Casertano, L. (1984). Intra-crater activity, a'a-block lava, viscosity and flow dynamics: Arenal Volcano, Costa Rica. *Journal of Volcanology and Geothermal Research*, *20*(1–2), 155–176. https://doi.org/10.1016/0377-0273(84)90072-6

Coombs, M. L., Bull, K. F., Vallance, J. W., Schneider, D. J., Thoms, E. E., Wessels, R. L., & McGimsey, R. G. (2010). Timing, distribution and volume of proximal products of the 2006 eruption of Augustine Volcano. *2006 Erupt. Augustine Volcano, Alaska*, 145–185.

Costa, A., Melnik, O., Sparks, R. S. J., & Voight, B. (2007). Control of magma flow in dykes on cyclic lava dome extrusion. *Geophysical Research Letters*, *34*, L02303. https://doi.org/10.1029/2006GL027466

Deardorff, N. D., & Cashman, K. V. (2012). Emplacement conditions of the c. 1,600-year BP Collier Cone lava flow, Oregon: A LiDAR investigation. *Bulletin of Volcanology*, *74*(9), 2051–2066. https://doi.org/10.1007/s00445-012-0650-9

Denlinger, R. P. (1997). A dynamic balance between magma supply and eruption rate at Kilauea volcano, Hawaii. *Journal of Geophysical Research*, *102*(B8), 18,091–18,100. https://doi.org/10.1029/97JB01071

Diefenbach, A. K., Bull, K. F., Wessels, R. L., & McGimsey, R. G. (2013). Photogrammetric monitoring of lava dome growth during the 2009 eruption of Redoubt Volcano. *Journal of Volcanology and Geothermal Research*, *259*, 308–316. https://doi.org/10.1016/j.jvolgeores.2011.12.009

Dieterich, J. H., & Decker, R. W. (1975). Finite element modeling of surface deformation associated with volcanism. *Journal of Geophysical Research*, *80*(29), 4094–4102. https://doi.org/10.1029/JB080i029p04094

Dietterich, H. R., Poland, M. P., Schmidt, D. A., Cashman, K. V., Sherrod, D. R., & Espinosa, A. T. (2012). Tracking lava flow emplacement on the east rift zone of Kīlauea, Hawai'i, with synthetic aperture radar coherence. *Geochemistry, Geophysics, Geosystems*, *13*, Q05001. https://doi.org/10.1029/2011GC004016

Dvorak, J. J., & Dzurisin, D. (1993). Variations in magma supply rate at Kīlauea Volcano, Hawai'i. *Journal of Geophysical Research*, *98*(B12), 22,255–22,268. https://doi.org/10.1029/93JB02765

Dvorak, J. J., & Okamura, A. T. (1987). In R. W. Decker, T. L. Wright, & P. H. Stauffer (Eds.), *Volcanism in Hawaii. US Geological Survey Professional Paper, 1350*, 1281–1296. https://pubs.usgs.gov/pp/1750/chapters/pp2008-1750_chapter08.pdf

Dzurisin, D. (2003). A comprehensive approach to monitoring volcano deformation as a window on the eruption cycle. *Reviews of Geophysics*, *41*, 1001. https://doi.org/10.1029/2003RG000134

Dzurisin, D. (2007). *Volcano deformation: Geodetic monitoring techniques* (Vol. xxxv, 441 pp.). Chichester, UK: Springer-Praxis. https://doi.org/10.1007/978-3-540-49302-0

Ebmeier, S., Biggs, J., Mather, T., Elliott, J., Wadge, G., & Amelung, F. (2012). Measuring large topographic change with InSAR: Lava thicknesses, extrusion rate and subsidence rate at Santiaguito volcano, Guatemala. *Earth and Planetary Science Letters*, *335-336*, 216–225. https://doi.org/10.1016/j.epsl.2012.04.027

Ebmeier, S. K., Biggs, J., Mather, T. A., & Amelung, F. (2013a). Applicability of InSAR to tropical volcanoes: Insights from Central America. *Geological Society London Special Publications*, *380*(1), 15–37. https://doi.org/10.1144/SP380.2

Ebmeier, S. K., Biggs, J., Mather, T. A., & Amelung, F. (2013b). On the lack of InSAR observations of magmatic deformation at Central American volcanoes. *Journal of Geophysical Research: Solid Earth*, *118*, 2571–2585. https://doi.org/10.1002/jgrb.50195

Ebmeier, S. K., Biggs, J., Muller, C., & Avard, G. (2014). Thin-skinned mass-wasting responsible for widespread deformation at Arenal volcano. *Frontiers of Earth Science*, *2*(December), 1–10. https://doi.org/10.3389/feart.2014.00035

Fink, J. H., & Griffiths, R. W. (1998). Morphology, eruption rates, and rheology of lava domes: Insights from laboratory models. *Journal of Geophysical Research*, *103*(B1), 527–545. https://doi.org/10.1029/97JB02838

Fournier, T. J., Pritchard, M. E., & Riddick, S. N. (2010). Duration, magnitude, and frequency of subaerial volcano deformation events: New results from Latin America using InSAR and a global synthesis. *Geochemistry, Geophysics, Geosystems*, *11*, Q01003. https://doi.org/10.1029/2009GC002558

Global Volcanism Program (2012). Report on Reventador (Ecuador) . In R. Wunderman (Ed.), *Bulletin of the Global Volcanism Network, 37:3*. Smithsonian Institution. https://doi.org/10.5479/si.GVP.BGVN201203-352010

Goldstein, R. M., & Werner, C. L. (1998). Radar interferogram filtering for geophysical applications. *Geophysical Research Letters*, *25*(21), 4035–4038. https://doi.org/10.1029/1998GL900033

González, P. J., Bagnardi, M., Hooper, A. J., Larsen, Y., Marinkovic, P., Samsonov, S. V., & Wright, T. J. (2015). The 2014–2015 eruption of Fogo volcano: Geodetic modeling of Sentinel-1 TOPS interferometry. *Geophysical Research Letters*, *42*, 9239–9246. https://doi.org/10.1002/2015GL066003

Gottsmann, J., Folch, A., & Rymer, H. (2006). Unrest at Campi Flegrei: A contribution to the magmatic versus hydrothermal debate from inverse and finite element modeling. *Journal of Geophysical Research*, *111*, B07203. https://doi.org/10.1029/2005JB003745

Gudmundsson, A. (2016). The mechanics of large volcanic eruptions. *Earth-Science Reviews*, *163*, 72–93. https://doi.org/10.1016/j.earscirev.2016.10.003

Gudmundsson, M. T., Jónsdóttir, K., Hooper, A., Holohan, E. P., Halldórsson, S. A., Ófeigsson, B. G., … Aiuppa, A. (2016). Gradual caldera collapse at Bárdarbunga volcano, Iceland, regulated by lateral magma outflow. *Science (80-.).*, *353*(6296), 1–24. https://doi.org/10.1126/science.aaf8988.sciencemag.org

Hall, M., Ramón, P., Mothes, P., LePennec, J. L., García, A., Samaniego, P., & Yepes, H. (2004). Volcanic eruptions with little warning: The case of Volcán Reventador's Surprise November 3, 2002 Eruption, Ecuador. *Revista geológica de Chile*, *31*(2), 349–358. https://doi.org/10.4067/S0716-02082004000200010

Harris, A. J., Rose, W. I., & Flynn, L. P. (2003). Temporal trends in lava dome extrusion at Santiaguito 1922–2000. *Bulletin of Volcanology*, *65*(2–3), 77–89. https://doi.org/10.1007/s00445-002-0243-0

Harris, A. J. L., Dehn, J., & Calvari, S. (2007). Lava effusion rate definition and measurement: A review. *Bulletin of Volcanology*, *70*(1), 1–22. https://doi.org/10.1007/s00445-007-0120-y

Harris, A. J. L., Murray, J. B., Aries, S. E., Davies, M. A., Flynn, L. P., Wooster, M. J., … Rothery, D. A. (2000). Effusion rate trends at Etna and Krafla and their implications for eruptive mechanisms. *Journal of Volcanology and Geothermal Research*, *102*(3–4), 237–270. https://doi.org/10.1016/S0377-0273(00) 00190-6

Hautmann, S., Hidayat, D., Fournier, N., Linde, A. T., Sacks, I. S., & Williams, C. P. (2013). Pressure changes in the magmatic system during the December 2008/January 2009 extrusion event at Soufrière Hills Volcano, Montserrat (W.I.), derived from strain data analysis. *Journal of Volcanology and Geothermal Research*, *250*, 34–41. https://doi.org/10.1016/j.jvolgeores.2012.10.006

Hickey, J., & Gottsmann, J. (2014). Benchmarking and developing numerical Finite Element models of volcanic deformation. *Journal of Volcanology and Geothermal Research*, *280*, 126–130. https://doi.org/10.1016/j.jvolgeores.2014. 05.011

Hooper, A., Pietrzak, J., Simons, W., Cui, H., Riva, R., Naeije, M., … Socquet, A. (2013). Importance of horizontal seafloor motion on tsunami height for the 2011 M_w = 9.0 Tohoku-Oki earthquake. *Earth and Planetary Science Letters*, *361*, 469–479. https://doi.org/10.1016/j.epsl.2012.11.013

Hreinsdóttir, S., Sigmundsson, F., Roberts, M. J., Björnsson, H., Grapenthin, R., Arason, P., … Óladóttir, B. A. (2014). Volcanic plume height correlated with magma-pressure change at Grímsvötn Volcano, Iceland. *Nature Geoscience*, *7*(3), 214–218. https://doi.org/10.1038/ngeo2044

Huppert, H. E., Shepherd, J. B., Haraldur Sigurdsson, R., & Sparks, S. J. (1982). On lava dome growth, with application to the 1979 lava extrusion of the Soufrière of St. Vincent. *Journal of Volcanology and Geothermal Research*, *14*(3–4), 199–222. https://doi.org/10.1016/0377-0273(82)90062-2

Huppert, H. E., & Woods, A. W. (2002). The role of volatiles in magma chamber dynamics. *Nature*, *420*(6915), 493–495. https://doi.org/10.1038/nature01211

Johnson, J. B., Lees, J. M., Gerst, A., Sahagian, D., & Varley, N. (2008). Long-period earthquakes and co-eruptive dome inflation seen with particle image velocimetry. *Nature*, *456*(7220), 377–381. https://doi.org/10.1038/nature07429

Jones, L. K., Kyle, P. R., Oppenheimer, C., Frechette, J. D., & Okal, M. H. (2015). Terrestrial laser scanning observations of geomorphic changes and varying lava lake levels at Erebus volcano, Antarctica. *Journal of Volcanology and Geothermal Research*, *295*, 43–54. https://doi.org/10.1016/j.jvolgeores.2015.02.011

Kelfoun, K., & Vallejo Vargas, S. (2015). VolcFlow capabilities and potential development for the simulation of lava flows. *Geological Society London Special Publications*, *426*(1), 337–343. https://doi.org/10.1144/SP426.8

Kozono, T., Ueda, H., Ozawa, T., Koyaguchi, T., Fujita, E., Tomiya, A., & Suzuki, Y. J. (2013). Magma discharge variations during the 2011 eruptions of Shinmoe-dake volcano, Japan, revealed by geodetic and satellite observations. *Bulletin of Volcanology*, *75*(3), 1–13. https://doi.org/10.1007/s00445-013-0695-4

Kubanek, J., Westerhaus, M., Schenk, A., Aisyah, N., Brotopuspito, K. S., & Heck, B. (2015). Volumetric change quantification of the 2010 Merapi eruption using TanDEM-X InSAR. *Remote Sensing of Environment*, *164*, 16–25. https://doi.org/10.1016/j.rse.2015.02.027

Lekner, J. (2007). Viscous flow through pipes of various cross-sections. *Journal of Physics*, *28*(3), 521–527. https://doi.org/10.1088/0143-0807/28/3/014

Lesher, C. E., & Spera, F. J. (2015). *Thermodynamic and Transport Properties of Silicate Melts and Magma, Encyclopedia of Volcanoes (Second Edition)* (chap. 5, pp. 113–141): Elsevier. https://doi.org/10.1016/B978-0-12-385938-9. 00005-5

Lu, Z., Masterlark, T., Dzurisin, D., Rykhus, R., & Wicks, C. (2003). Magma supply dynamics at Westdahl volcano, Alaska, modeled from satellite radar interferometry. *Journal of Geophysical Research Earth*, *108*(B7), 2354. https://doi.org/10.1029/2002JB002311

Manen Van, S. M., Dehn, J., & Blake, S. (2010). Satellite thermal observations of the Bezymianny lava dome 1993–2008: Precursory activity, large explosions, and dome growth. *Journal of Geophysical Research*, *115*, B08205. https://doi.org/10.1029/2009JB006966

Massonnet, D., & Feigl, K. L. (1998). Radar interferometry and its application to changes in the Earth's surface. *Reviews of Geophysics*, *36*(4), 441. https://doi.org/10.1029/97RG03139

Mastin, L., Roeloffs, E., & Beeler, N. (2008). Constraints on the size, overpressure, and volatile content of the Mount St. Helens magma system from geodetic and dome-growth measurements during the 2004–2006+ eruption, ch. 22. In D. R. Sherrod, W. E. Scott, & P. H. Stauffer (Eds.), *A Volcano Rekindled: The renewed eruption of Mount St. Helens, 2004–2006. U.S. Geological Survey*. 461–488. https://pubs.usgs.gov/pp/1750/chapters/pp2008-1750_ chapter22.pdf

Mastin, L. G., Lisowski, M., Roeloffs, E., & Beeler, N. (2009). Improved constraints on the estimated size and volatile content of the Mount St. Helens magma system from the 2004–2008 history of dome growth and deformation. *Geophysical Research Letters*, *36*, L20304. https://doi.org/10.1029/2009GL039863

McCormick-Kilbride, B., Edmonds, M., & Biggs, J. (2016). Observing eruptions of gas-rich compressible magmas from space. *Nature Communications*, *7*(13), 744. https://doi.org/10.1038/ncomms13744

McTigue, D. F. (1987). Elastic stress and deformation near a finite spherical magma body: Resolution of the point source paradox. *Journal of Geophysical Research*, *92*(B12), 12,931–12,940. https://doi.org/10.1029/JB092iB12p12931

Melnik, O., & Sparks, R. S. J. (2005). Controls on conduit magma flow dynamics during lava dome building eruptions. *Journal of Geophysical Research*, *110*, B02209. https://doi.org/10.1029/2004JB003183

Miller, T. P. (1994). Dome growth and destruction during the 1989–1990 eruption of Redoubt volcano. *Journal of Volcanology and Geothermal Research*, *62*(1–4), 197–212. https://doi.org/10.1016/0377-0273(94) 90034-5

Mogi, K. (1958). Relations between the eruptions of various volcanoes and the deformations of the ground surfaces around them. *Bulletin of the Earthquake Research Institute*, *36*, 99–134. https://doi.org/10.1016/j.epsl.2004.04.016

Moran, S. C., Kwoun, O., Masterlark, T., & Lu, Z. (2006). On the absence of InSAR-detected volcano deformation spanning the 1995–1996 and 1999 eruptions of Shishaldin Volcano, Alaska. *Journal of Volcanology and Geothermal Research*, *150*(1–3), 119–131. https://doi.org/10.1016/j.jvolgeores.2005.07.013

Mosegaard, K., & Tarantola, A. (1995). Monte Carlo sampling of solutions to inverse problems. *Journal of Geophysical Research*, *100*(B7), 12,431–12,447. https://doi.org/10.1029/94JB03097

Nakada, S., Shimizu, H., & Ohta, K. (1999). Overview of the 1990–1995 eruption at Unzen Volcano. *Journal of Volcanology and Geothermal Research*, *89*(1–4), 1–22. https://doi.org/10.1016/S0377-0273(98) 00118-8

Naranjo, M. F. (2013). Estudio petro-geoquímico y cronológico de los flujos de lava emitidos por el volcán Reventador entre 2002 a 2009 (Masters thesis). Escuela Politécnica Nacional. http://bibdigital.epn.edu.ec/handle/15000/6443

Naranjo, J. A., Sparks, R. S. J., Stasiuk, M. V., Moreno, H., & Ablay, G. J. (1992). Morphological, structural and textural variations in the 1988–1990 andesite lava of Lonquimay volcano, Chile. *Geological Magazine*, *129*(6), 657–678. https://doi.org/10.1017/S0016756800008426

Naranjo, M. F., Ebmeier, S. K., Vallejo, S., Ramón, P., Mothes, P., Biggs, J., & Herrera, F. (2016). Mapping and measuring lava volumes from 2002 to 2009 at El Reventador Volcano, Ecuador, from field measurements and satellite remote sensing. *Journal of Applied Volcanology*, *5*(1), 8. https://doi.org/10.1186/s13617-016-0048-z

Navarro-Ochoa, C., Gavilanes-Ruíz, J. C., & Cortés-Cortés, A. (2002). Movement and emplacement of lava flows at Volcán de Colima, México: November 1998-February 1999. *Journal of Volcanology and Geothermal Research*, *117*(1–2), 155–167. https://doi.org/10.1016/S0377-0273(02)00242-1

Nomikou, P., Parks, M. M., Papanikolaou, D., Pyle, D. M., Mather, T. A., Carey, S., … Perros, I. (2014). The emergence and growth of a submarine volcano: The Kameni islands, Santorini (Greece). *GeoResJ*, *1–2*, 8–18. https://doi.org/10.1016/j.grj.2014.02.002

Okada, Y. (1985). Surface deformation due to shear and tensile faults in a half-space. *International Journal of Rock Mechanics and Mining Sciences Geomechanics Abstracts*, *75*(4), 1135–1154. https://doi.org/10.1016/0148-9062(86)90674-1

Pallister, J. S., Schneider, D. J., Griswold, J. P., Keeler, R. H., Burton, W. C., Noyles, C., … Ratdomopurbo, A. (2013). Merapi 2010 eruption-Chronology and extrusion rates monitored with satellite radar and used in eruption forecasting. *Journal of Volcanology and Geothermal Research*, *261*, 144–152. https://doi.org/10.1016/j.jvolgeores.2012.07.012

Peltier, A., Bachèlery, P., & Staudacher, T. (2009). Magma transport and storage at Piton de La Fournaise (La Réunion) between 1972 and 2007: A review of geophysical and geochemical data. *Journal of Volcanology and Geothermal Research*, *184*(1–2), 93–108. https://doi.org/10.1016/j.jvolgeores.2008.12.008

Pinel, V., Hooper, A., De la Cruz-Reyna, S., Reyes-Davila, G., Doin, M., & Bascou, P. (2011). The challenging retrieval of the displacement field from InSAR data for andesitic stratovolcanoes: Case study of Popocatepetl and Colima Volcano, Mexico. *Journal of Volcanology and Geothermal Research*, *200*(1–2), 49–61. https://doi.org/10.1016/j.jvolgeores.2010.12.002

Pinel, V., Poland, M., & Hooper, A. (2014). Volcanology: Lessons learned from synthetic aperture radar imagery. *Journal of Volcanology and Geothermal Research*, *289*, 81–113. https://doi.org/10.1016/j.jvolgeores.2014.10.010

Poland, M. P. (2014). Time-averaged discharge rate of subaerial lava at Kīlauea Volcano, Hawai'i, measured from TanDEM-X interferometry: Implications for magma supply and storage during 2011-2013. *Journal of Geophysical Research: Solid Earth*, *119*, 5464–5481. https://doi.org/10.1002/2014JB011132

Poland, M. P., Miklius, A., Jeff Sutton, A., & Thornber, C. R. (2012). A mantle-driven surge in magma supply to Kīlauea Volcano during 2003–2007. *Nature Geoscience*, *5*(4), 295–300. https://doi.org/10.1038/ngeo1426

Pritchard, M. E., & Simons, M. (2002). A satellite geodetic survey of large-scale deformation of volcanic centres in the central Andes. *Nature*, *418*(6894), 167–71. https://doi.org/10.1038/nature00872

Ratdomopurbo, A., Beauducel, F., Subandriyo, J., Agung Nandaka, I. G. M., Newhall, C. G., Suharna, D. S., … Sunarta (2013). Overview of the 2006 eruption of Mt. Merapi. *Journal of Volcanology and Geothermal Research*, *261*, 87–97. https://doi.org/10.1016/j.jvolgeores.2013.03.019

Reverso, T., Vandemeulebrouck, J., Jouanne, F., Pinel, V., Villemin, T., Sturkell, E., & Bascou, P. (2014). A two-magma chamber model as a source of deformation at Grímsvötn Volcano, Iceland. *Journal of Geophysical Research: Solid Earth*, *119*, 4666–4683. https://doi.org/10.1002/2013JB010569

Ridolfi, F., Puerini, M., Renzulli, A., Menna, M., & Toulkeridis, T. (2008). The magmatic feeding system of El Reventador volcano (Sub-Andean zone, Ecuador) constrained by texture, mineralogy and thermobarometry of the 2002 erupted products. *Journal of Volcanology and Geothermal Research*, *176*(1), 94–106. https://doi.org/10.1016/j.jvolgeores.2008.03.003

Rivalta, E., & Segall, P. (2008). Magma compressibility and the missing source for some dike intrusions. *Geophysical Research Letters*, *35*, L04306. https://doi.org/10.1029/2007GL032521

Rivera Morales, A. M., Amelung, F., & Mothes, P. (2016). Volcano deformation survey over the Northern and Central Andes with ALOS InSAR time series. *Geochemistry, Geophysics, Geosystems*, *17*, 2869–2883. https://doi.org/10.1002/2016GC006393

Rymer, H., & Williams-Jones, G. (2000). Volcanic eruption prediction: Magma chamber physics from gravity and deformation measurements. *Geophysical Research Letters*, *27*(16), 2389–2392. https://doi.org/10.1029/1999GL011293

Salzer, J. T., Nikkhoo, M., Walter, T. R., Sudhaus, H., Reyes-Dávila, G., Bretón, M., & Arámbula, R. (2014). Satellite radar data reveal short-term pre-explosive displacements and a complex conduit system at Volcán de Colima, Mexico. *Frontiers of Earth Science*, *2*(June), 1–11. https://doi.org/10.3389/feart.2014.00012

Samaniego, P., Eissen, J. P., Le Pennec, J. L., Robin, C., Hall, M. L., Mothes, P., … Cotten, J. (2008). Pre-eruptive physical conditions of El Reventador volcano (Ecuador) inferred from the petrology of the 2002 and 2004–05 eruptions. *Journal of Volcanology and Geothermal Research*, *176*(1), 82–93. https://doi.org/10.1016/j.jvolgeores.2008.03.004

Sanderson, R. W., Johnson, J. B., & Lees, J. M. (2010). Ultra-long period seismic signals and cyclic deflation coincident with eruptions at Santiaguito volcano, Guatemala. *Journal of Volcanology and Geothermal Research*, *198*(1–2), 35–44. https://doi.org/10.1016/j.jvolgeores.2010.08.007

Scandone, R. (1979). Effusion rate and energy balance of Paricutin eruption (1943–1952), Michoacan, Mexico. *Journal of Volcanology and Geothermal Research*, *6*(1–2), 49–59. https://doi.org/10.1016/0377-0273(79) 90046-5

Scharff, L., Ziemen, F., Hort, M., Gerst, A., & Johnson, J. B. (2012). A detailed view into the eruption clouds of Santiaguito volcano, Guatemala, using Doppler radar. *Journal of Geophysical Research*, *117*, B04201. https://doi.org/10.1029/2011JB008542

Schilling, S. P., Thompson, R., Messerich, J., & Iwatsubo, E. Y. (2008). Use of digital aerophotogrammetry to determine rates of lava dome growth, Mount St. Helens, Washington, 2004–2005, ch. 8. In D. R. Sherrod, W. E. Scott, & P. H. Stauffer (Eds.), *A Volcano Rekindled Renewed Erupt. Mt. St. Helens 2004–2006. U.S. Geological Survey Professional Paper, 1750*, 145–167. https://pubs.usgs.gov/pp/1750/chapters/pp2008-1750_chapter08.pdf

Segall, P. (2005). *Earthquake and volcano deformation* (517 pp.). Princeton, NJ: Princeton University Press. https://doi.org/10.1002/0471743984.vse7429

Segall, P. (2013). Volcano deformation and eruption forecasting. *Geological Society London Special Publications*, *380*(1), 85–106. https://doi.org/10.1144/SP380.4

Segall, P., Cervelli, P., Owen, S., Lisowski, M., & Miklius, A. (2001). Constraints on dike propagation from continuous GPS measurements. *Journal of Geophysical Research*, *106*(B9), 19,301–19,317. https://doi.org/10.1029/2001JB000229

Sheldrake, T. E., Sparks, R. S. J., Cashman, K. V., Wadge, G., & Aspinall, W. P. (2016). Similarities and differences in the historical records of lava dome-building volcanoes: Implications for understanding magmatic processes and eruption forecasting. *Earth-Science Reviews*, *160*, 240–263. https://doi.org/10.1016/j.earscirev.2016.07.013

Simkin, T., Siebert, L., McClelland, L., Bridge, D., Newhall, C., & Latter, J. H. (1981). *Volcanoes of the world: A regional directory, gazetteer, and chronology of volcanism during the last 10,000 years* (Vol. viii, 232 pp.). New York: Hutchinson Ross Pub Co.

Siswowidjoyo, S., Suryo, I., & Yokoyama, I. (1995). Magma eruption rates of Merapi volcano, Central Java, Indonesia during one century (1890–1992). *Bulletin of Volcanology*, *57*(2), 111–116. https://doi.org/10.1007/BF00301401

Sparks, R. S. J. (1997). Causes and consequences of pressurisation in lava dome eruptions. *Earth and Planetary Science Letters*, *150*(3–4), 177–189. https://doi.org/10.1016/S0012-821X(97)00109-X

Sparks, R. S. J., & Aspinall, W. P. (2004). Volcanic activity: Frontiers and challenges in forecasting, prediction and risk assessment. *The State of the Planet: Frontiers and Challenges in Geophysics, Geophysical Monograph Series*, *150*, 359–373. https://doi.org/10.1029/150GM28

Sparks, R. S. J., Young, S. R., Barclay, J., Calder, E. S., Cole, P., Darroux, B., … Watts, R. (1998). Magma production and growth of the lava dome of the Sourfriere Hills Volcano, Montserrat, West Indies: November 1995 to December 1997. *Geophysical Research Letters*, *25*, 3421–3424. https://doi.org/10.1029/98GL00639

Swanson, D. A., & Holcomb, R. T. (1990). Regularities in growth of the Mount St. Helens Dacite Dome, 1980–1986, *Lava Flows Domes* (Vol. 2, pp. 3–24). Berlin Heidelberg: Springer. https://doi.org/10.1007/978-3-642-74379-5

Thouret, J.-C. (1999). Volcanic geomorphology—An overview. *Earth-Science Reviews*, *47*(1), 95–131. https://doi.org/10.1016/S0012-8252(99)00014-8

Vallejo Vargas, S., Kelfoun, K., Diefenback, A., Ramon, P., Vasconez, F., Naranjo, M. F., & Pino, G. (2015). Numerical simulations of lava flows. A calibration from thermal images of lava emplacement at El Reventador volcano, *poster presented at 26th Int. Union Geol. Geophys. Gen. Assem.*Prague. 22 June–2 July 2015. http://www.researchgate.net/publication/294729286_Vallejo_et_al_IUGG-2015

Voight, B., Hoblitt, R. P., Clarke, A. B., Lockhart, A. B., Miller, A. D., Lynch, L., & McMahon, J. (1998). Remarkable cyclic ground deformation monitored in real-time on Montserrat, and its use in eruption forecasting. *Geophysical Research Letters*, *25*(18), 3405–3408. https://doi.org/10.1029/98GL01160

Wadge, G. (1981). The variation of magma discharge during basaltic eruptions. *Journal of Volcanology and Geothermal Research*, *11*(2–4), 139–168. https://doi.org/10.1016/0377-0273(81)90020-2

Wadge, G. (1982). Steady state volcanism: Evidence from eruption histories of polygenetic volcanoes. *Journal of Geophysical Research*, *87*(B5), 4035–4049. https://doi.org/10.1029/JB087iB05p04035

Wadge, G. (1983). The magma budget of Volcan Arenal, Costa Rica from 1968 to 1980. *Journal of Volcanology and Geothermal Research*, *19*(3–4), 281–302. https://doi.org/10.1016/0377-0273(83)90115-4

Wadge, G., Cole, P., Stinton, A., Komorowski, J.-C., Stewart, R., Toombs, A., & Legendre, Y. (2011). Rapid topographic change measured by high-resolution satellite radar at Sourfrière Hills Volcano, Montserrat, 2008–2010. *Journal of Volcanology and Geothermal Research*, *199*(1–2), 142–152. https://doi.org/10.1016/j.jvolgeores.2010.10.011

Wadge, G., Herd, R., Ryan, G., Calder, E. S., & Komorowski, J.-C. (2010). Lava production at Soufrière Hills Volcano, Montserrat: 1995–2009. *Geophysical Research Letters*, *37*, L00E03. https://doi.org/10.1029/2009GL041466

Wadge, G., Oramas Dorta, D., & Cole, P. (2006). The magma budget of Volcán Arenal, Costa Rica from 1980 to 2004. *Journal of Volcanology and Geothermal Research*, *157*(1–3), 60–74. https://doi.org/10.1016/j.jvolgeores.2006.03.037

Wadge, G., Mattioli, G., & Herd, R. (2006). Ground deformation at Soufrière Hills Volcano, Montserrat during 1998–2000 measured by radar interferometry and GPS. *Journal of Volcanology and Geothermal Research*, *152*(1–2), 157–173. https://doi.org/10.1016/j.jvolgeores.2005.11.007

Wadge, G., Scheuchl, B., & Stevens, N. F. (2002). Spaceborne radar measurements of the eruption of Sourfrière Hills Volcano, Montserrat. *Geological Society, London, Memoirs*, *21*(1), 583–594. https://doi.org/10.1144/GSL.MEM. 2002.021.01.27

Wadge, G., Voight, B., Sparks, R. S. J., Cole, P. D., Loughlin, S. C., & Robertson, R. E. A. (2014). Chapter 1 An overview of the eruption of Soufriere Hills Volcano, Montserrat from 2000 to 2010. *Geological Society, London, Memoirs*, *39*(1), 1–40. https://doi.org/10.1144/M39.1

Wadge, G., Macfarlane, D. G., Odbert, H. M., Stinton, A., Robertson, D. A., James, M. R., & Pinkerton, H. (2014). Chapter 13 AVTIS observations of lava dome growth at Soufriere Hills Volcano, Montserrat: 2004 to 2011. *Geological Society, London, Memoirs*, *39*(1), 229–240. https://doi.org/10.1144/M39.13

Walker, G. P. L., Huntingdon, A. T., Sanders, A. T., & Dinsdale, J. L. (1973). Lengths of lava flows [and discussion]. *Philosophical Transactions of the Royal Society A: Mathematical, Physical, and Engineering Sciences*, *274*(1238), 107–118. https://doi.org/10.1098/rsta.1973.0030

Walter, T. R., Legrand, D., Granados, H. D., Reyes, G., & Arámbula, R. (2013). Volcanic eruption monitoring by thermal image correlation: Pixel offsets show episodic dome growth of the Colima volcano. *Journal of Geophysical Research: Solid Earth*, *118*, 1408–1419. https://doi.org/10.1002/jgrb.50066

Watts, R. B., Herd, R. A., Sparks, R. S. J., & Young, S. R. (2002). Growth patterns and emplacement of the andesitic lava dome at Sourfrière Hills Volcano, Montserrat. *Geological Society, London, Memoirs*, *21*(1), 115–152. https://doi.org/10.1144/GSL.MEM.2002.021.01.06

Werner, C., Wegmüller, U., Strozzi, T., & Wiesmann, A. (2000). Gamma SAR and interferometric processing software. In *Proceedings of the ERS-Envisat Symposium*, Gothenburg, Sweden. Retrieved from http://citeseerx.ist.psu.edu/viewdoc/summary?doi=10.1.1.20.6363

Werner, C., Wegmüller, U., Strozzi, T., & Wiesmann, A. (2002). Processing strategies for phase unwrapping for INSAR applications. *Proc. of EUSAR 2002 - 4th European Conference on Synthetic Aperture Radar*, *1*, 353–356.

Woods, A. W., & Huppert, H. E. (2003). On magma chamber evolution during slow effusive eruptions. *Journal of Geophysical Research*, *108*(B8), 2403. https://doi.org/10.1029/2002JB002019

Woods, A. W., & Koyaguchi, T. (1994). Transitions between explosive and effusive eruptions of silicic magmas. *Nature*, *370*(6491), 641–644. https://doi.org/10.1038/370641a0

Wright, R. (2016). MODVOLC: 14 years of autonomous observations of effusive volcanism from space. *Geological Society London Special Publications*, *426*(1), 23–53. https://doi.org/10.1144/SP426.12

Xu, W., & Jónsson, S. (2014). The 2007–8 volcanic eruption on Jebel at Tair island (Red Sea) observed by satellite radar and optical images. *Bulletin of Volcanology*, *76*(2), 795. https://doi.org/10.1007/s00445-014-0795-9

Yang, X.-M., Davis, P. M., & Dieterich, J. H. (1988). Deformation from inflation of a dipping finite prolate spheroid in an elastic half-space as a model for volcanic stressing. *Journal of Geophysical Research*, *93*(B5), 4249–4257. https://doi.org/10.1029/JB093iB05p04249

Zharinov, N. A., & Demyanchuk, Y. V. (2008). The growth of an extrusive dome on Shiveluch Volcano, Kamchatka in 1980–2007: Geodetic observations and video surveys. *Journal of Volcanology and Seismology*, *2*(4), 217–227. https://doi.org/10.1134/S0742046308040015